Inorganic Chemistry

pubs.acs.org/IC

Article

N,C,N-Pincers in Platinum Bimetallic Complexes: Influence of the Pincer and Bridging Ligands on the Metal−Metal Bond and the Photophysical Properties

Miguel A. Esteruelas,* Sonia Moreno-Blázquez, Montserrat Oliván, and Enrique Oñate

Cite This: *Inorg. Chem.* 2024, 63, 14482−14494

Read Online

ACCESS | Metrics & More | Article Recommendations | Supporting Information

ABSTRACT: Precursors PtCl{κ^3-*N,C,N*-[py-C_6HMe_2-py]} (**1**), PtCl{κ^3-*N,C,N*-[py-O-C_6H_3-O-py]} (**2**), Pt(OH){κ^3-*N,C,N*-[py-C_6HMe_2-py]} (**3**), and Pt(OH){κ^3-*N,C,N*-[py-O-C_6H_3-O-py]} (**4**) were used to prepare d^8-platinum bimetallic complexes. Precursors **1** and **2** react with $AgBF_4$ and 7-azaindole (H*az*) to give [Pt{κ^3-*N,C,N*-[py-C_6HMe_2-py]}{κ^1-*N*-[H*az*]}]BF_4 (**5**) and [Pt{κ^3-*N,C,N*-[py-O-C_6H_3-O-py]}{κ^1-*N*-[H*az*]}]BF_4 (**6**) and **3** and **4** with indolo[2,3-*b*]indole (H_2*ii*) to generate Pt{κ^1-*N*-[H*ii*]}{κ^3-*N,C,N*-[py-C_6HMe_2-py]} (**7**) and Pt{κ^1-*N*-[H*ii*]}{κ^3-*N,C,N*-[py-O-C_6H_3-O-py]} (**8**). Subsequent addition of **3** and **4** to **5**-**7** affords bimetallic derivatives [{Pt[κ^3-*N,C,N*-(py-C_6HMe_2-py)]}$_2${μ-*N,N*-[*az*]}]BF_4 (**9**), [{Pt[κ^3-*N,C,N*-(py-O-C_6H_3-O-py)]}$_2${μ-*N,N*-[*az*]}]BF_4 (**10**), and {Pt[κ^3-*N,C,N*-(py-C_6HMe_2-py)]}$_2${μ-*N,N*-[*ii*]} (**11**). X-ray structures of **9**-**11** reveal separations between the metals in sequence **9** (3.0515(4) Å) < **10** (3.2689(9) Å) < **11** (3.2949(2) Å). DFT calculations support σ overlap of the dz^2 orbitals of platinum atoms, for **9** and **10**. Accordingly, their absorption spectra show a MMLCT transition. Complex **9** is a red emitter. The excited state has ^{3}MMLCT characteristics and a Pt−Pt separation of 2.763 Å. Complex **11** is a dual emitter in the red and NIR regions, in solid. Both excited states have a ^{3}LC/LMCT characteristic and platinum−platinum separations of 3.290 and 3.202 Å. Intermediate **5** is a green emitter that achieves quantum yields close to unity, when diluted in PMMA and 1,2-dichloroethane at low concentrations.

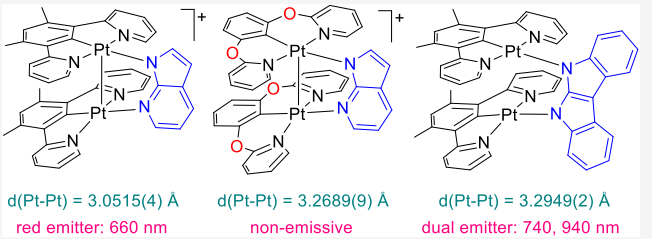

INTRODUCTION

There is great interest in controlling the separation between the metal centers of d^8-platinum bimetallic complexes. The interest is mainly motivated by the influence that this parameter has on the photophysical properties of these complexes. The relatively large Pt−Pt separations provide little interaction between the metals. As a consequence, dimeric species emit similarly to mononuclear subunits, with excited states resulting from the combination of metal-to-ligand charge transfer (MLCT) and ligand-centered (LC) transitions. In contrast, short Pt−Pt distances provide strong dz^2-dz^2 interactions, causing a sharp split between the generated molecular orbitals, dσ-bonding and dσ*-antibonding. The splitting produces an increase in the energy of the HOMO, which is centered on dσ*. Thus, excited states are best described as a metal−metal-to-ligand charge transfer (MMLCT).[1]

The most common designs have been structures of the types [Pt{κ^2-*C,N*-[chelate]}(μ-L_2)]$_2$ and [Pt{(κ^2-*C,C*-[chelate]}(μ-L_2)]$_2$. The first type is based on two platinum subunits, which contain an orthometalated phenyl-*N*-heterocycle, linked by a double bridge formed by two bidentate ligands resulting from the deprotonation of molecules type: thiazolthiol,[2] quinolinyl- and pyridylthiol,[3] hydroxyquinoline,[4] hydroxypyridine,[5] pyrazol,[6] triazole,[7] and terminal alkyne.[8] The second one is constructed in a similar way, changing the *N*-donor heterocycle by an NHC group and using pyrazolate[9] or formamidinate[10] as bridges. The separation between the platinum centers is usually governed by the bridging ligands, giving rise to two class of structures: rigid and flexible. Bridges built on anionic *N,S*- and *N,O*-donor ligands derived from thiazolthiol, quinolinyl- and pyridylthiol, hydroxyquinoline and hydroxypyridine produce rigid structures with short metal−metal distances, leading to strong ^{3}MMLCT emissions. Because dσ* is antibonding in character, photoexcitation produces a T_1 structure that exhibits additional contraction of the Pt−Pt distance.[2,3,4,5] On the other hand, the double pyrazolate bridges generate flexible structures that allow access to a wide range of Pt−Pt separations, both in the ground state and in the excited state. The separation between the metals can be adjusted by modifying the volume of the pyrazolate substituents. Due to the flexibility of the double bridge, the emitters that produce ^{3}MMLCT emissions undergo an ultrafast photoinduced structural change, in solution, which generates two conformational isomeric structures of T_1, with

Received: April 26, 2024
Revised: June 28, 2024
Accepted: July 4, 2024
Published: July 19, 2024

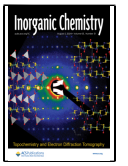

https://doi.org/10.1021/acs.inorgchem.4c01712
Inorg. Chem. 2024, 63, 14482−14494

Scheme 1. Preparation of the New Complexes

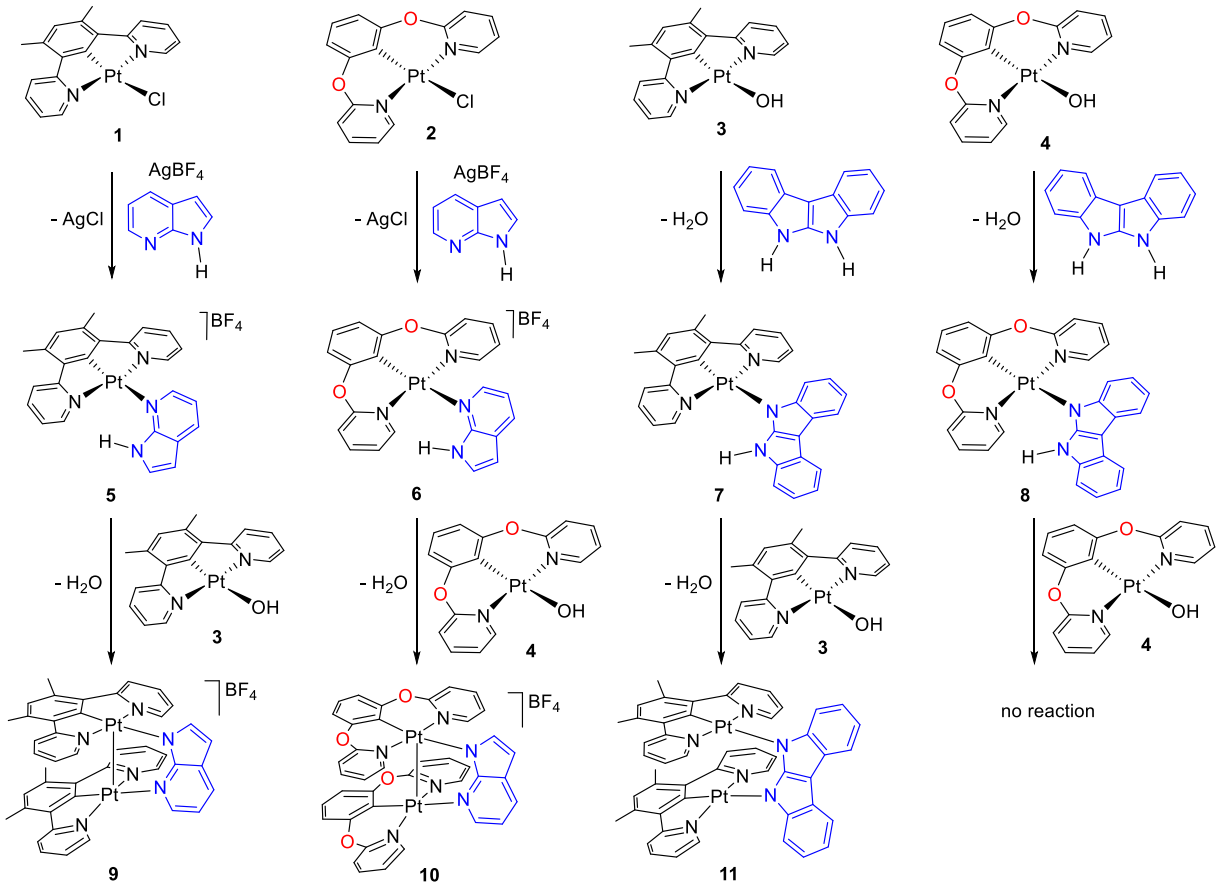

long and short metal−metal separations, giving rise to a dual emission.[6c,9b] That is, each isomer produces its own emission, the excited state with a longer Pt−Pt separation at higher energy and the excited state with a shorter Pt−Pt distance at lower energy. The chelating group of platinum subunits also appears to play some role in controlling Pt−Pt separation, although its effect has been much less studied. A recent analysis in a family of complexes containing phenyl-pyridine-type orthometalated groups in platinum subunits linked by two 2-mercaptobenzothiazole *N,S*-bridges points out that an increase in the electron deficiency of the *C,N*-ligand results in an increase of π-back-donation from the filled dxy orbital of platinum to the empty π^* orbital of the heterocycle. This causes a reduction in the electronic repulsion of the partially overlapping dxz orbitals, which leads to the shortening of the Pt−Pt distance.[11]

Pincer ligands are gaining importance as tools to stabilize phosphorescent emitters that provide special characteristics.[12] However, its use to construct d^8-platinum bimetallic complexes has been scarce, mainly limited to terpyridine type ligands[13] and 6-phenyl-2,2′-bipyridine type pro-ligands.[14] These pincers result in Pt{κ^3-*N,N,X*-[pincer]} subunits, which form the compounds $[\{Pt[\kappa^3\text{-}N,N,X\text{-}(pincer)]\}_2(\mu\text{-}L_2)]^{n+}$ (X = N, C; n = 3, 2, 1) when joined by a diphosphine,[14a,b,d,e] bis(NHC),[14c] *N*-heterocycle-thiolate,[13b,c,e] pyrazolate,[13a,d] or acetylide[13f,g] monobridge. The Pt−Pt separation in these cations is usually longer than in complexes containing subunits with bidentate ligands, probably due to the greater flexibility of the monobridge. As a consequence, emissions ^{3}MMLCT have rarely been observed.[15]

The *N,C,N*-ligands occupy a prominent position among the pincers.[16] In particular, those generated by the activation of the C−H bond at the 2-position of the central ring of 1,3-di(2-pyridyl)benzene-type pro-ligands and related molecules attract increasing interest in platinum(II) chemistry.[17] In this context, we have recently studied the conflict posed by the joint coordination, to platinum(II), of ligands such as 1,3-bis(2-pyridyl)-4,6-dimethylphenyl- or 1,3-bis(2-pyridyloxy)phenyl and chelating groups of the type 3-(2-pyridyl)-pyrazolate, seeking to analyze the influence of typical parameters of pincer ligands, including bite angle, hemilability, and electron delocalization capacity, on the emissive properties of the resulting metals species. The results indicate that the pincer coordination of 1,3-bis(2-pyridyl)-4,6-dimethylphenyl is stronger than that of 1,3-bis(2-pyridyloxy)phenyl. Although the presence of oxygen atoms between the phenyl and pyridyl groups in the latter allows a more comfortable arrangement of the donor atoms, from a geometric point of view, they prevent the electron delocalization within the generated metallaheterocycles. Such delocalization in 1,3-bis(2-pyridyl)-4,6-dimethylphenyl derivatives favors the pincer coordination of the tridentate ligand, compensating and overcoming the increase in comfort provided by the oxygen atoms of 1,3-bis(2-pyridyloxy)phenyl. Complexes containing the pincer ligand 1,3-bis(2-pyridyl)-4,6-dimethylphenyl and κ^1-N^1-pyridylpyrazolate-type groups are among the most efficient platinum(II) green phosphorescent emitters.[18]

We are now interested in obtaining information on how the metal−metal bond of bimetallic d^8-platinum complexes can be governed with *N,C,N*-pincer ligands. In particular we wish to know the influence of the presence of oxygen atoms between the phenyl and pyridyl groups of 1,3-di(2-pyridyl)phenyl type

https://doi.org/10.1021/acs.inorgchem.4c01712
Inorg. Chem. 2024, 63, 14482−14494

ligands. To do this, we have generated Pt{κ^3-*N,C,N*-[pincer]} subunits, with the pincer ligands 1,3-di(2-pyridyl)-4,6-dimethylphenyl and 1,3-bis(2-pyridyloxy)phenyl, which are linked with *N,N*-monobridges resulting from the deprotonation of the 7-azaindole (H*az*) and indolo[2,3-*b*]indole (H_2*ii*) pro-ligands. These *N,N*-monobridges provide more rigid dimeric structures than those generated by pyrazolate or diphosphine.[19] This article describes the sequence of events that lead to complexes of type $[\{Pt[\kappa^3\text{-}N,C,N\text{-(pincer)}]\}_2(\mu\text{-}N{-}N)]^{n+}$ (n = 1, 0), with the mentioned ligands. In addition, it analyzes structurally and using DFT methods the Pt−Pt bond and the influence that this parameter has on the photophysical properties of the new complexes.

RESULTS AND DISCUSSION

Preparation and Structural Characterization of the New Complexes. Scheme 1 summarizes the synthetic procedures leading to the designed $[\{Pt[\kappa^3\text{-}N,C,N\text{-(pincer)}]\}_2(\mu\text{-N-N})]^{n+}$ compounds. They are based on the use of the chloride precursors PtCl{κ^3-*N,C,N*-[py-C_6HMe_2-py]} (**1**) and PtCl{κ^3-*N,C,N*-[py−O-C_6H_3−O-py]} (**2**) and their hydroxide derivatives Pt(OH){κ^3-*N,C,N*-[py-C_6HMe_2-py]} (**3**) and Pt(OH){κ^3-*N,C,N*-[py-O-C_6H_3-O-py]} (**4**) and develop through mononuclear intermediates [Pt{κ^3-*N,C,N*-[py-C_6HMe_2-py]}{κ^1-*N*-[H*az*]}]BF_4 (**5**), [Pt{κ^3-*N,C,N*-[py-O-C_6H_3-O-py]}{κ^1-*N*-[H*az*]}]BF_4 (**6**), Pt{κ^1-*N*-[H*ii*]}{κ^3-*N,C,N*-[py-C_6HMe_2-py]} (**7**) and Pt{κ^1-*N*-[H*ii*]}{κ^3-*N,C,N*-[py-O-C_6H_3-O-py]} (**8**). Salts **5** and **6** were generated by abstraction of the chloride ligand from precursors **1** and **2** with $AgBF_4$, in acetone, and subsequent coordination of the H*az* ligand; they were isolated as pale yellow and white solids, respectively, with almost quantitative yields (≈95%). Molecular species **7** and **8** result from the coordinative deprotonation of one of the N−H groups of pro-ligand H_2*ii*, promoted by the hydroxide ligand of complexes **3** and **4**; they were isolated as orange and yellow solids with yields of 50% and 60%, respectively. The most notable spectroscopic characteristics of these intermediates are a ν(N−H) band between 3300 and 3430 cm^{-1}, in the IR; a broad singlet due to the NH-hydrogen atom, in the range 7.90−9.90 ppm, in the ^{1}H NMR spectra; and a singlet between −3100 and −3800 ppm in the ^{195}Pt{^{1}H} NMR spectra. The treatment of salts **5** and **6**, in acetone, at room temperature, with the hydroxide precursors **3** and **4** produces the substitution of the NH-hydrogen atom of the ligand H*az*, by the corresponding subunit Pt{κ^3-*N,C,N*-[pincer]}, with release of water. The substitution gives rise to the respective bimetallic salts $[\{Pt[\kappa^3\text{-}N,C,N\text{-(py-}C_6HMe_2\text{-py)}]\}_2\{\mu\text{-}N,N\text{-}[az]\}]BF_4$ (**9**) and $[\{Pt[\kappa^3\text{-}N,C,N\text{-(py-O-}C_6H_3\text{-O-py)}]\}_2\{\mu\text{-}N,N\text{-}[az]\}]BF_4$ (**10**), which were isolated as red and yellowish-white solids, respectively, in yields of approximately 65%. The inequivalent ^{195}Pt nuclei of these salts generate two signals between −3000 and −3600 ppm, in the ^{195}Pt{^{1}H} NMR spectra. Under the same conditions, the reaction of **7** with **3** leads to the bimetallic species $\{Pt[\kappa^3\text{-}N,C,N\text{-(py-}C_6HMe_2\text{-py)}]\}_2\{\mu\text{-}N,N\text{-}[ii]\}$ (**11**), in the form of a blood-red solid in almost quantitative yield. This complex is completely insoluble in common organic solvents. Unlike **7**, complex **8** is completely inert in the presence of **4**. It was impossible to prepare a bimetallic compound similar to **11** with the ligand 1,3-bis(2-pyridyloxy)phenyl.

Figure 1 shows a view of the cation of **5**.[20] The coordination around the platinum(II) center is the usual square-planar arrangement, with the central aryl group of the pincer and the H*az* ligand disposed in trans. As expected, the Pt−N_{pincer} distances of 2.015(3) and 2.025(3) Å (Pt−N(3) and Pt−N(4), respectively) are significantly shorter (about 0.11 Å) than the Pt−N_{Haz} (Pt−N(1)) bond length of 2.136(3) Å. The molecules stack through $\pi-\pi$ interactions between the rings of the *N,C,N*-ligands (Figure S29a),[21] which were confirmed by using an AIM approach (Figure S30). Two cations with alternating orientation associate to form a pair through the interaction of the aryl linker of a pincer with the pyridyl ring of the other. The separation between the centroids of the rings involved is 3.8279(2) Å, whereas the separation between the platinum atoms is 7.6242(5) Å. The pairs are associated with other pairs above and below, using the aryl group and a pyridyl ring; the separation between pairs is 3.9301(2) Å. The interacting rings are slightly displaced, with slips in the offset conformation in the range 1.57−2.16 Å.

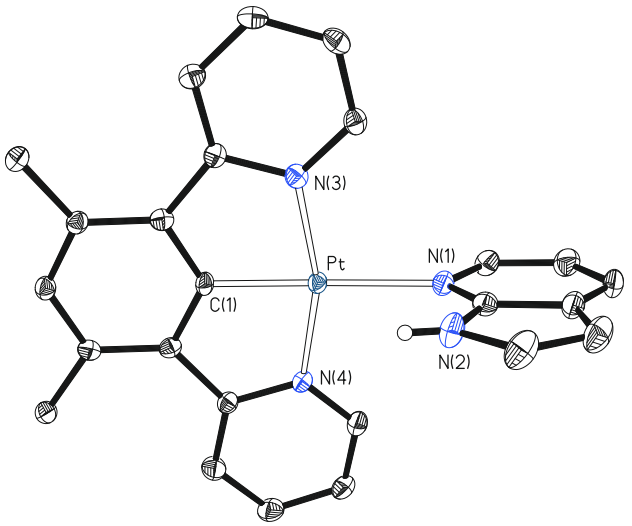

Figure 1. X-ray structure of the cation of complex **5** (displacement ellipsoids shown at 50% probability). All hydrogen atoms (except the NH) are omitted for clarity. Selected bond distances (Å) and angles (deg): Pt−C(1) = 1.924(3), Pt−N(1) = 2.136(3), Pt−N(3) = 2.015(3), Pt−N(4) = 2.025(3); N(3)−Pt−N(4) = 162.41(12), N(3)−Pt−C(1) = 81.46(13), N(4)−Pt−C(1) = 81.03(13), C(1)−Pt−N(1) = 176.96(12), N(1)−Pt−N(3) = 97.83(11), N(1)−Pt−N(4) = 99.74(11).

Complex **7** was also characterized by X-ray diffraction analysis. Figure 2 shows the molecular structure. The geometry around the metal center resembles that of **5** with the H*ii* ligand in the H*az* group position. The anionic character of the H*ii* ligand appears to shorten the platinum-monodentate ligand distance. Thus, the Pt−N_{Hii} bond length, 2.018(8) Å (Pt−N(1)), is slightly shorter than the Pt−N_{Haz} distance. Two molecules of **7** with alternate orientation associate to form pairs analogous to those of **5** (Figure S29b), the separation between molecules being 3.950(2) Å; about 0.12 Å longer than in **5**. However, unlike the latter, pairs of **7** do not undergo association with other pairs. The higher steric requirement of H*ii* with respect to H*az* might explain the difference.

Dimers **9**−**11** were also characterized by X-ray diffraction analysis, to perform a comparative structural analysis on the influence of the pincer and bridging ligands on the metal−metal separation. Figure 3 shows the structures (a−c, respectively), whereas Table 1 summarizes the main structural parameters. The structures conform to what was designed. Thus, they can be described as nearly parallel square planar subunits, stabilized by an *N,C,N*-pincer ligand, which are linked by a *N,N*-bridging

https://doi.org/10.1021/acs.inorgchem.4c01712
Inorg. Chem. 2024, 63, 14482−14494

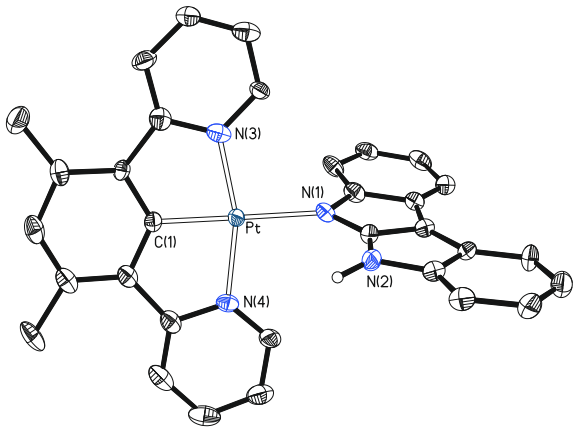

Figure 2. X-ray structure of complex **7** (displacement ellipsoids shown at 50% probability). All hydrogen atoms (except the NH) are omitted for clarity. Selected bond distances (Å) and angles (deg): Pt−C(1) = 1.863(9), Pt−N(1) = 2.018(8), Pt−N(3) = 1.980(8), Pt−N(4) = 1.915(8); N(3)−Pt−N(4) = 162.9(3), N(3)−Pt−C(1) = 78.2(4), N(4)−Pt−C(1) = 84.7(4), C(1)−Pt−N(1) = 178.5(4), N(1)−Pt−N(3) = 102.5(3), N(1)−Pt−N(4) = 94.6(3).

ligand. The main conclusion derived from their comparison is that the separation between the metals depends equally on both the pincer and the bridging ligand. The cation of **9** (a) shows a Pt−Pt distance of 3.0515(4) Å, suggesting strong metal−metal bonding. Replacing the 1,3-di(2-pyridyl)-4,6-dimethylphenyl pincer with 1,3-bis(2-pyridyloxy)phenyl produces a significant elongation of approximately 0.22 Å of the Pt−Pt distance. Such elongation points to a marked destabilization of the metal−metal bond in **10** (b) with respect to **9**. The reason seems to be related to the flexibility that the oxygen atoms bring to the structure of the subunits and the repulsion they experience when one is on top of the other. As a result, the **10** subunits are wavy rather than flat. The replacement of the monoanionic bridge *az* in **9** by the dianionic bridge ligand *ii* also leads to a notable elongation of the distance between the metals, almost 0.30 Å. Thus, the metal−metal separation in the molecular species **11** (c) of 3.2949(2) Å is comparable to the separation observed at **10**, 3.2689(9) Å. As expected, 1,3-di(2-pyridyl)-4,6-dimethylphenyl coordinates with angles that deviate markedly from the ideal values of 90° and 180°, while the 1,3-bis(pyridyloxy)-phenyl ligand allows angles close to ideal values. Despite this, the lengths of the platinum−nitrogen and platinum−carbon bonds are very similar in the three compounds.[18]

Absorption Spectra, Frontier Orbitals and Electrochemical Properties. Figures S31−S36 show the UV−vis spectra of 10^{-5} M solutions of **5**−**10**, in 1,2-dichloroethane, at room temperature, whereas Figure S37 presents the diffuse reflectance spectrum of a 4% solid solution of **11** in $BaSO_4$. Because the cations of **5** in the solid state associate through $\pi-\pi$ interactions, the spectrum of this salt was also studied as a function of concentration, at 390 nm, ensuring compliance with Beer's law in the concentration range $5.56 \times 10^{-6} - 1.00 \times 10^{-4}$ M, while for higher concentrations it clearly deviates (Figure S38). Spectra in 1,2-dichloroethane were calculated by TD-DFT (B3LYP-D3//SDD(f)/6-31G**); Figures S31−S37 give those obtained, while Tables S1−S8 gather the transitions that contribute to the bands. Figures S39−S45 group the most relevant orbitals, whereas Tables S8−S14 list the fragments involved in said orbitals.

Table 2 collects some relevant absorptions and their assignment. The bands observed for the mononuclear species **5**−**8** are due to metal-to-pincer combined with intra- and interligand charge transfers. The very weak tails at the end of the spectra involve formal spin-forbidden transitions, which result from the large spin−orbit coupling provided by platinum. The spectra of bimetallic complexes **9** and **10** are similar to those of mononuclear compounds **5** and **6** with a very notable difference; the presence of weak absorptions ($\varepsilon \approx 3697$ (**9**), 9800 (**10**) $M^{-1} \cdot cm^{-1}$), at about 490 nm for **9** and at about 350 nm for **10**. They correspond to transitions HOMO−LUMO almost pure (97%). For both complexes, the HOMO is mainly localized on the metals (39% and 42% for **9** and 35% and 40% for **10**), while the LUMO mainly lies on the pyridinic rings of the pincer ligand (39% and 32% for **9** and 54% and 37% for **10**). Therefore, these absorptions correspond to MMLCT transitions. Being characteristic of a Pt−Pt bond in bimetallic complexes,[22] the energy increases as the metal−metal bond weakens. Unlike **9** and **10**, the calculated spectrum of **11** does not contain any transition showing pure MMLCT character, suggesting that 3.2949(2) Å is too long a distance to support a true Pt−Pt bonding.

Figure 4 shows the frontier orbitals of mononuclear complexes **5**−**7** and bimetallic compounds **9**−**11**. The HOMO of **5** is centered on the platinum center (24%) and the pincer ligand (74%), with an almost negligible participation of the monodentate group. The contribution of the latter to the HOMO of **6** increases significantly to 22% at the expense of the pincer. In contrast, the HOMO of **7** is practically centered on the monodentate ligand (97%). The LUMO of the three mononuclear species is mainly situated on the pyridine rings of the pincers with a small contribution from the aryl linker and

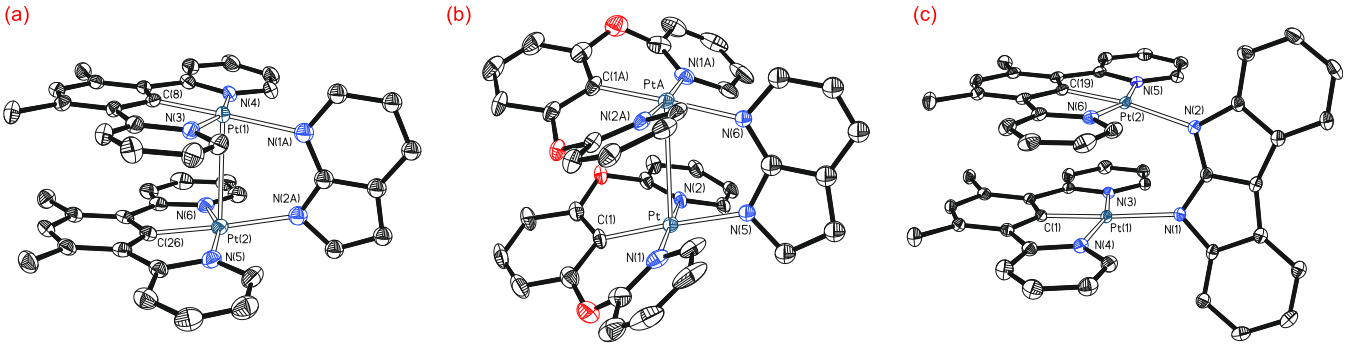

Figure 3. X-ray structures of the cations of complexes **9** (a), **10** (b) and of complex **11** (c) (displacement ellipsoids shown at 50% (**9** and **11**) and 30% (**10**) probability). Hydrogen atoms are omitted for clarity.

https://doi.org/10.1021/acs.inorgchem.4c01712
Inorg. Chem. 2024, 63, 14482−14494

Table 1. Selected Bond Distances (Å) and Angles (deg) in the X-ray Structures of Complexes 9, 10, and 11

distances and angles	9	10	11
Pt−Pt	3.0515(4)	3.2689(9)	3.2949(2)
$Pt-C_{pincer}$	1.924(4), 1.920(4)	1.977(13), 1.977(13)	1.926(2), 1.919(2)
$Pt-N_{pincer}$	2.024(4), 2.022(4), 2.018(4), 2.019(4)	2.036(11), 2.038(13), 2.036(11), 2.038(13)	2.018(2), 2.019(2), 2.011(2), 2.015(2)
$Pt-N_{lig}$	2.179(3), 2.110(6)	2.096(12), 2.097(11)	2.122(2), 2.109(2)
$N_{pincer}-Pt-N_{pincer}$	162.04(15), 161.63(15)	174.6(5), 174.6(5)	161.37(8), 161.85(9)
$N_{pincer}-Pt-C_{pincer}$	80.78(17), 80.98(17), 81.17(17), 81.39(17)	88.2(5), 88.9(6), 88.2(5), 88.9(6)	80.76(10), 80.77(10), 80.90(10), 81.25(10)
$C_{pincer}-Pt-N_{lig}$	176.6(2), 176.9(2)	173.9(6), 175.0(7)	172.32(9), 176.77(9)

Table 2. Selected Calculated (TD-DFT in 1,2-Dichloroethane) and Experimental UV−Vis Absorptions for 5−11 (in 1,2-Dichloroethane) and their Major Contributions

λ exp (nm)	ϵ (M^{-1} cm^{-1})	exc. energy (nm)	oscillator strength, f	excited state character
complex **5**				
267	18 527	262	0.4771	HOMO−1 → LUMO+4 (79%)
390	4223	355	0.1450	HOMO → LUMO+1 (95%)
440	26	470 (T_1)	0	HOMO → LUMO (46%) HOMO−1 → LUMO+1 (38%)
complex **6**				
236	39 200	248	0.1449	HOMO−1 → LUMO+4 (46%) HOMO−1 → LUMO+6 (10%)
316	11 900	324	0.0465	HOMO → LUMO (95%)
388	100	412 (T_1)	0	HOMO−2 → LUMO+1 (24%) HOMO−2 → LUMO+2 (24%) HOMO → LUMO+1 (13%) HOMO → LUMO+2 (14%)
complex **7**				
268	62 700	263	0.3453	HOMO−4 → LUMO+3 (63%) HOMO−3 → LUMO+3 (16%)
380	9200	363	0.0944	HOMO−2 → LUMO+1 (61%) HOMO−4 → LUMO (25%)
593	200	598 (T_1)	0	HOMO → LUMO (98%)
complex **8**				
269	48 900	249	0.1389	HOMO−4 → LUMO+2 (26%) HOMO−4 → LUMO+3 (20%) HOMO−3 → LUMO+2 (20%)
324	24 400	323	0.0421	HOMO−2 → LUMO (68%) HOMO−1 → LUMO+2 (15%)
489	200	501 (T_1)	0	HOMO → LUMO (99%)
complex **9**				
293	39 221	295	0.2011	HOMO−7 → LUMO+1 (67%)
492	3697	475	0.0740	HOMO → LUMO (97%)
565	114	516 (T_1)	0	HOMO → LUMO (95%)
complex **10**				
233	84 000	269	0.1685	HOMO−6 → LUMO+4 (44%) HOMO → LUMO+9 (13%)
351	9800	387	0.0316	HOMO → LUMO (97%)
435	100	434 (T_1)	0	HOMO−1 → LUMO+4 (50%) HOMO−1 → LUMO+3 (17%)
complex **11**				
397		377	0.1263	HOMO−4 → LUMO+1 (43%) HOMO−3 → LUMO+1 (30%) HOMO−2 → LUMO+1 (19%)
496		431	0.0462	HOMO−2 → LUMO (67%) HOMO−3 → LUMO (24%)
687		721 (T_1)	0	HOMO → LUMO (99%)

the metal center. The HOMO of bimetallic complexes **9** and **10** is dσ* ($5dz^2-5dz^2$); the antibonding molecular orbital resulting from the σ overlap of the dz^2 orbitals of the two platinum atoms. However, the HOMO of **11** is centered on the bridging ligand; that is, the same place as in the mononuclear precursor. As in the mononuclear species, the LUMO of the three bimetallic compounds is located mainly in the pyridine rings of the pincer ligand. The calculated HOMO−LUMO gap is significantly larger in mononuclear compounds than in bimetallic complexes. It depends on both the pincer ligand and the bridging-bidentate or monodentate group, while it does not seem to have a clear relationship with the separation between platinum atoms in bimetallic compounds; the complex with the longest separation displays the smallest HOMO−LUMO gap. 1,3-Bis(2-pyridyloxy)phenyl generates larger gaps than 1,3-di(2-pyridyl)-4,6-dimethylphenyl, while H*ii* and *ii* generate smaller gaps than H*az* and *az*. Thus, the gaps decrease according to the sequences **6** > **5** > **7** and **10** > **9** > **11**.

The redox properties of the soluble mononuclear and bimetallic complexes were evaluated by cyclic voltammetry, to also have experimental information on the frontier orbitals. The measurements were carried out in an argon atmosphere, in 1,2-dichloroethane, at room temperature, using $[Bu_4N]PF_6$ as a supporting electrolyte (0.1 M). Figures S46−S51 provide views of the voltammograms. Salts **5**, **6**, **9**, and **10** present two irreversible oxidations, $[M]^+/[M]^{2+}$ and $[M]^{2+}/[M]^{3+}$ or $[M_2]^+/[M_2]^{2+}$ and $[M_2]^{2+}/[M_2]^{3+}$, and two irreversible reductions, $[M]^+/[M]$ and $[M]/[M]^-$ or $[M_2]^+/[M_2]$ and $[M_2]/[M_2]^-$, while molecular species **7** and **8** undergo two reversible oxidations, $[M]/[M]^+$ and $[M]^+/[M]^{2+}$, and two irreversible reductions, $[M]/[M]^-$ and $[M]^-/[M]^{2-}$. Table 3 lists the potential values against Fc/Fc^+, which are in the range of −0.27 to 0.90 V for oxidations and between −0.85 and −1.75 V for reductions. Table 3 also contains the HOMO energy levels estimated from the first oxidation potentials and the LUMO energy levels estimated from the first reduction potentials, as

https://doi.org/10.1021/acs.inorgchem.4c01712
Inorg. Chem. 2024, 63, 14482−14494

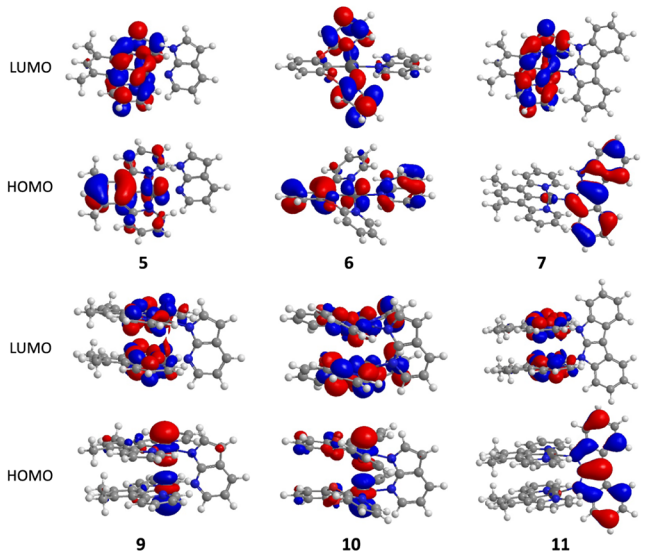

Figure 4. Frontier orbitals of mononuclear complexes **5**−**7** and bimetallic compounds **9**−**11** (isovalue 0.03 au).

well as the HOMO and LUMO energy levels calculated by DFT. There is good qualitative agreement between the HOMO−LUMO gap estimated from the experimental potential values and those calculated by DFT. As deduced from the DFT calculations, the experimentally estimated gap values indicate that 1,3-bis(2-pyridyloxy)phenyl generates higher gap values than 1,3-di(2-pyridyl)-4,6-dimethylphenyl, while H*ii* gives rise to smaller gaps than H*az*.

Emissive Properties. Both the pincer ligand and the bridging-bidentate or monodentate group govern the emissive properties of the new prepared compounds. This was expected, since both influence the structure, nature, and HOMO−LUMO gap of the resulting compounds. The pincer ligand determines the planar or wavy shape of the square-planar units and dictates the degree of aggregation between cations or molecules. For its part, the bridging-bidentate or monodentate group decides the saline or molecular nature of the generated species. The separation between platinum atoms in bimetallic species is also conditioned by both. Table 4 summarizes of most relevant emissive findings of the new compounds. All measurements were performed under argon.

Salt **5** has a cation bearing the pincer ligand 1,3-di(2-pyridyl)-4,6-dimethylphenyl and the monodentate group H*az*. In agreement with the ability of this cation to undergo aggregation, it is a self-quenching emissive material, upon photoexcitation. Thus, its emissive properties depend on the measurement medium and the concentration of salt in the medium. At 298 K, the spectrum of a poly(methyl methacrylate) film containing 5 wt % of salt ($PMMA_{5\%}$) shows a highly structured emission in the green region of the spectrum, between 490 and 590 nm, and a very broad band centered around 640 nm. Dilution of the salt up to 2 wt % ($PMMA_{2\%}$) leads to a significant decrease in the intensity of the structureless broad band in the red region (Figure 5a). Furthermore, the quantum yield experiences a dramatic increase from 0.58 to 0.96. At the same temperature, the spectra of solutions between 1×10^{-6} and 1×10^{-3} M in 1,2-dichloroethane are similar to the spectra in the PMMA films, although the intensity of the unstructured band is lower and decreases as the concentration of emitter also diminishes (Figure 5b). Like for the films, the quantum yield gradually raises from 0.40 to almost 1 as the dilution increases. In frozen 1,2-dichloroethane matrices at 77 K, the spectra show a dramatic increase of the unstructured band in the red region at the expense of the green emission (Figure 5c). The green emission comes from the excited state T_1, which possesses a significant ligand-centered $^3\pi-\pi^*$ character. This origin is supported by the excellent agreement between the wavelength of the structured band maximum and the calculated value for the energy difference between the optimized T_1 triplet state and the S_0 singlet state. The broad band in the red region stems from aggregates with excimeric character,[17c,n,23] which quench the green emission. Consistent with this, the excitation spectra monitored at the red emission maximum show an MMLCT band centered at approximately 470 nm, which is not observed in the excitation spectra monitored at the green emission maximum (Figure S62). The replacement of 1,3-di(2-pyridyl)-4,6-dimethylphenyl by 1,3-bis(2-pyridyloxy)phenyl prevents self-quenching, as expected from the low inclination of the resulting cation to aggregate. Thus, salt **6** is a poor green emitter ($\Phi_L < 0.03$) that displays emissions independent of salt concentration, both in PMMA film and in 1,2-dichloroethane (Figure S63). A similar effect as a consequence of the same pincer substitution was recently observed in related neutral emitters.[18] The interchange of the neutral monodentate group H*az* by the anionic monodentate ligand H*ii* does not change the emissive characteristics provided by the pincer, but drastically reduces the efficiency of the emitter. Like **5**, molecular complex **7** is a green emitter, which undergoes self-quenching (Figure S72), but only achieves maximum quantum yields of approximately 0.09 (Table 4). The 1,3-bis(2-pyridyloxy)phenyl counterpart **8** is nonemissive. Consistent with the narrowing of the HOMO−LUMO gap in the sequence **6** > **5** > **7**, the maximum of the green emission shows a red shift in the opposite direction.

The bimetallic salt **9** is also an emitter; its emissive properties however show significant differences from those of mononuclear

Table 3. Electrochemical and DFT Molecular Orbitals Energy Data for 5−10

			Obs (eV)					Calcd (eV)		
complex	E_{ox} (V)[a]	E_{red} (V)[a]	HOMO[b]	LUMO[b]	E_{00}[c]	LUMO from E_{00}[d]	HLG[e]	HOMO	LUMO	HLG[e]
5	0.24, 0.65	−1.09, −1.66	−5.04	−3.71	2.63	−2.41	1.33	−6.15	−2.14	4.01
6	0.45, 0.90	−1.40, −1.65	−5.25	−3.40	2.90	−2.35	1.85	−6.32	−1.81	4.51
7	−0.27[f], 0.11[f]	−1.12, −1.75	−4.53	−3.68	2.65	−1.88	0.85	−4.42	−1.82	2.6
8	−0.22[f], 0.63[f]	−1.07, −1.73	−4.58	−3.73	2.67	−2.33	0.85	−4.49	−1.48	3.01
9	0.28, 0.61	−0.85, −1.53	−5.08	−3.95	2.17	−1.91	1.13	−5.56	−2.20	3.36
10	0.25, 0.81[f]	−1.05, −1.68	−5.05	−3.75	2.72	−2.33	1.30	−5.72	−1.82	3.9

[a]Measured under argon in 1,2-dichloroethane/$[Bu_4N]PF_6$ (0.1 M), vs Fc/Fc^+. [b]HOMO = −[E_{ox} vs Fc/Fc^+ + 4.8] eV; LUMO = −[E_{red} vs Fc/Fc^+ + 4.8] eV. [c]E_{00} = onset of emission. [d]LUMO from E_{00} = HOMO + E_{00}. [e]HLG = LUMO − HOMO. [f]$E_{ox1/2}$.

https://doi.org/10.1021/acs.inorgchem.4c01712
Inorg. Chem. 2024, 63, 14482−14494

Table 4. Selected[a] Photophysical Data for Complexes 5, 6, 7, 9, and 11

calc λ_{em}(nm)	medium	T (K)	concentration	λ_{em}(nm)[b]	τ_{av}(μs) green-shifted band[c]	τ_{av}(μs) red-shifted band[c]	τ_{av}(μs) NIR-shifted band[c]	Φ_L[d]
Complex **5**								
	PMMA	298	2% weight	**490**, 524, 560, 640	11.63 (83.5%), 5.35 (16.5%)	10.81 (12.3%), 2.67 (87.7%)		0.96
495	$C_2H_4Cl_2$	298	1×10^{-5} M	**490**, 524, 560, 640	13.67 (89.3%), 5.89 (10.7%)			0.97
	$C_2H_4Cl_2$	77	1×10^{-5} M	490, 524, **640**	11.53 (62.1%), 4.59 (37.9%)	7.37 (15.5%), 3.59 (84.5%)		
Complex **6**								
	PMMA	298	5% weight	458, **488**, 520	393.60 (33.2%), 119.20 (66.8%)			0.01
467	$C_2H_4Cl_2$	298	1×10^{-5} M	**494**, 554, 568	12.91			0.03
Complex **7**								
	PMMA	298	2% weight	494, 528, **620**	3.31 (55.9%), 1.07 (44.1%)	0.76 (28.4%), 0.27 (71.6%)		0.08
691	$C_2H_4Cl_2$	298	1×10^{-5} M	**494**, 528, 570	4.57			0.09
	$C_2H_4Cl_2$	77	1×10^{-5} M	**492**, 528, 570, 650	8.78	2.97 (46.8%), 0.94 (53.2%)		
Complex **9**								
	PMMA	298	2% weight	660		2.15		0.46
623	$C_2H_4Cl_2$	298	1×10^{-5} M	494, 528, **670**	5.08	1.96		0.50
Complex **11**								
738, 918	solid	298	2% weight	712, **917**			0.08	0.004
	solid	77	2% weight	734, **917**			0.31 (78.4%), 0.001 (21.6%)	

[a]Table 4 summarizes the data in Table S15. [b]The most intense peak is in bold. [c]Relative amplitudes (%) are given in parentheses for biexponential decays. [d]Absolute quantum yield.

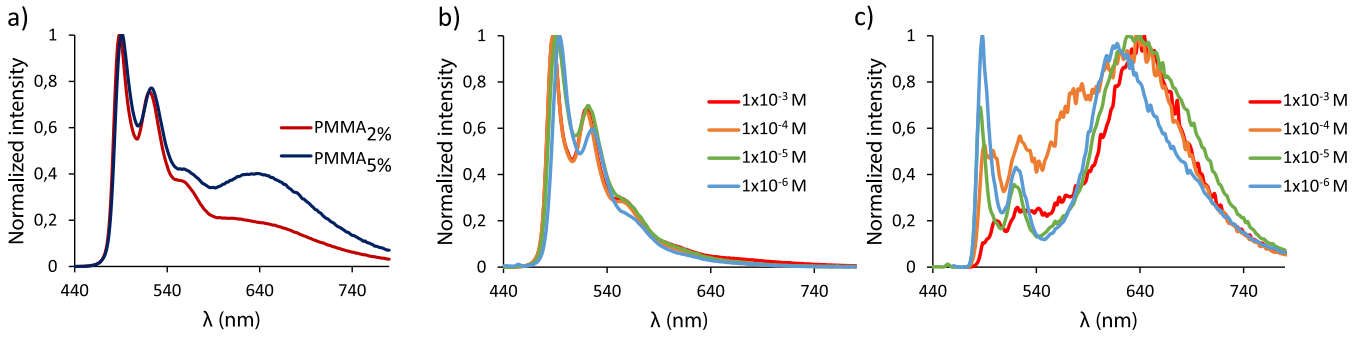

Figure 5. Emission spectra of complex **5** in (a) PMMA films at 298 K, (b) 1,2-dichloroethane solutions at 298 K, and (c) in frozen matrices of 1,2-dichloroethane at 77 K.

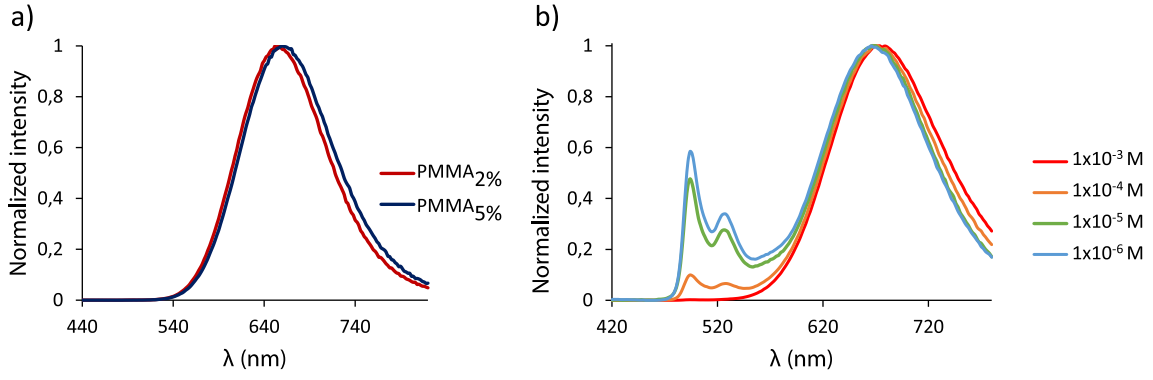

Figure 6. Emission spectra of complex **9** in (a) PMMA films at 298 K and (b) in 1,2-dichloroethane solutions at 298 K.

compounds **5**–**7**. At 298 K, the spectra of poly(methyl methacrylate) films doped with 2 and 5 wt % salt contain only one concentration-independent unstructured band in the red region, centered around 660 nm, upon excitation at 400 nm (Figure 6a). The emission shows a quantum yield of 0.46. Under the same photoexcitation, the emission spectra of the salt, in 1,2-dichloroethane, at room temperature depend on the concentration, showing the unstructured band in the red region and a

https://doi.org/10.1021/acs.inorgchem.4c01712
Inorg. Chem. 2024, 63, 14482−14494

weak and highly structured green emission with a maximum at 496 nm, which increases in intensity as the dilution increases (Figure 6b). Substitution of 1,3-di(2-pyridyl)-4,6-dimethylphenyl by 1,3-bis(2-pyridyloxy)phenyl quenches the emission as in the mononuclear salts. In contrast to **9**, the salt **10** practically does not emit.

The excitation spectrum of a 1×10^{-6} M solution of **9**, in 1,2-dichloroethane, monitored at the intense red emission maximum resembles the absorption spectrum, including the MMLCT band at approximately 490 nm. On the contrary, the latter disappears when the excitation spectrum is monitored at the green emission maximum (Figure 7).

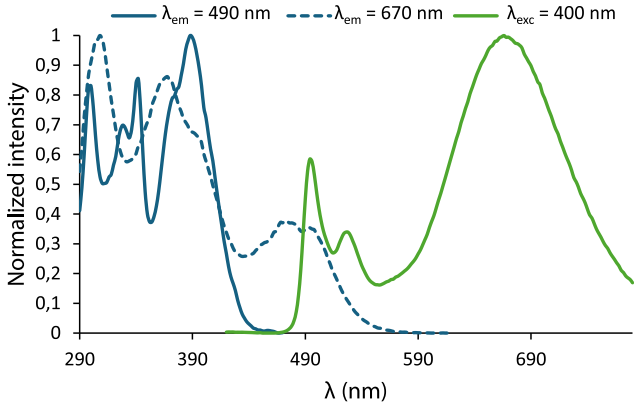

Figure 7. Normalized excitation (λ_{em} = 670 nm, blue dotted line; λ_{em} = 490 nm, blue line) and emission (λ_{ex} = 400 nm, green line) spectra of a 1×10^{-6} M solution in 1,2-dichloroethane of complex **9**.

The red emission stems from a T_1 excited state with ^{3}MMLCT characteristic and a short Pt−Pt distance of 2.763 Å; Figure 8a shows a plot of its spin density calculated by DFT. This origin is strongly supported by the very good agreement between the wavelength of the emission maxima and the calculated values for the energy differences between the optimized triplet state and the singlet state S_0. The green emission appears to result from the deformation of the bimetallic structure of the emitter as a consequence of the inclusion of a solvent molecule between the monomeric subunits. The pyridyl groups of the pincer ligand anchor a solvent molecule through Cl−π interactions.[24] The introduction of the solvent causes separation of the metal centers up to 3.488 Å, which prevents any MMLCT transition. Thus, we find an energy minimum corresponding to the optimized structure of an S_0' state with these characteristics (Figure S138), which is approximately 1−2 kcal mol^{-1} less stable than the structure of S_0 plus a molecule of 1,2-dichloroethane. The emission estimated from the T_1' state with said geometry by TD-DFT, 476 nm, agrees well with that observed experimentally.

Molecular bimetallic complex **11** is a weak dual emitter ($\Phi_L \approx 0.004$) in the solid state, at 298 and 77 K, after photoexcitation at λ = 520 nm. Under these conditions, the spectra of the pure solid and of the solid solutions containing 5 and 2% by weight of the complex in SiO_2 contain two unstructured bands, one of them in the red region, centered at approximately 740 nm, and the other in the NIR region, centered at 918 nm (Figures S89−S91). Such wavelengths compare remarkably well with the values calculated for the energy differences between the optimized excited states T_{1b} and T_{1c} (Figure 8b,c) and the singlet state S_0. Triplets T_{1b} and T_{1c} originate from HOMO−LUMO and HOMO−1−LUMO transitions, respectively. Since HOMO and HOMO−1 are centered on the bridging ligand (98 and 92%) and LUMO on the pincer (86%) and metal centers (7 and 7%), both excited states have ^{3}LC/LMCT characteristic. From a geometric point of view, they are conformers of S_0, with separations between the metals similar to that found in the ground state; 3.290 and 3.202 Å. The excited state T_{1b} provides the red emission and is 7.6 kcal mol^{-1} above the excited state T_{1c} which is responsible for the NIR band. The photoinduced structural change to transform T_{1b} and T_{1c} must exceed a very low activation energy of 0.2 kcal mol^{-1}. To our knowledge, complex **11** is the first dual emitter in solid-state.

CONCLUDING REMARKS

This study reveals the procedure to prepare complexes of type $[\{Pt[\kappa^3\text{-}N,C,N\text{-}(pincer)]\}_2(\mu\text{-}N{-}N)]^{n+}$ (n = 1, 0), with the pincer ligands 1,3-di(2-pyridyl)-4,6-dimethylphenyl and 1,3-bis(2-pyridyloxy)phenyl and the anionic bridging groups *az* (H*az* = 7-azaindole) and *ii* (H$_2$*ii* = indolo[2,3-*b*]indole), shows the influence of the pincer ligand and the bridging group on the platinum−platinum separation, and provides the photophysical properties of the new synthesized species.

The strategy designed to obtain the desired complexes is developed in two steps and requires the use of two different precursors; PtCl{[κ^3-*N,C,N*-[pincer]} and Pt(OH){[κ^3-*N,C,N*-[pincer]}. It starts from the X-precursors (X = Cl, OH), which generate mononuclear intermediates [Pt{κ^3-*N,C,N*-[pincer]}-(N-NH)]$^{n+}$ (n = 1, 0) in the first step. The reaction of these

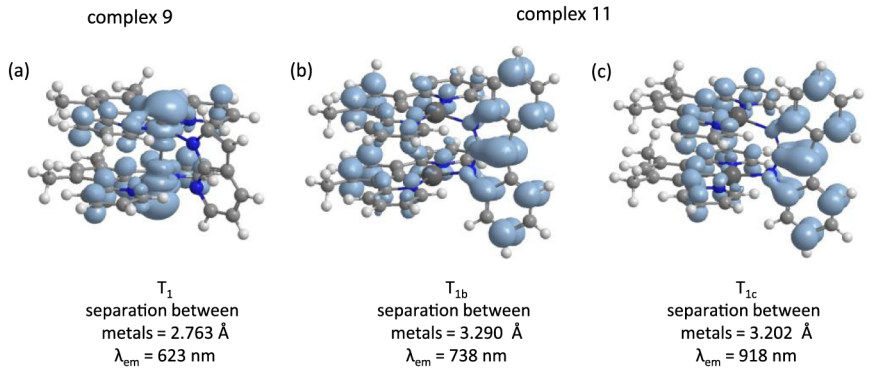

Figure 8. DFT calculated spin density for the triplet states T_1 (a) of complex **9** and for the triplet states T_{1b} (b) and T_{1c} (c) of complex **11** at 0.002 au contour level.

https://doi.org/10.1021/acs.inorgchem.4c01712
Inorg. Chem. 2024, 63, 14482−14494

intermediates with the OH-precursors produces the planned compounds.

The X-ray diffraction analysis structures of these bimetallic complexes points out that the separation between metals depends on both the pincer ligand and the bridging group. The 1,3-bis(2-pyridyloxy)phenyl pincer lengthens the separation by approximately 7% with respect to 1,3-di(2-pyridyl)-4,6-dimethylphenyl, whereas the *ii* bridge lengthens it by approximately 10% compared to *az*. In this context, DFT calculations show that the HOMO of the complexes bearing the *az* bridge corresponds to the antibonding molecular orbital resulting from the σ overlap of the dz^2 orbitals of the two platinum atoms, while the HOMO of the compounds carrying bridge *ii* is in the bridging ligand. This is supported experimentally by the absorption spectra, which display clear MMLCT transitions for the first ones. Both the DFT calculations and the electrochemical study of the compounds furthermore indicate that the HOMO−LUMO gap depends on both the pincer ligand and the bridging group, while it does not seem to have a clear relationship with the separation between platinum atoms. 1,3-Bis(2-pyridyloxy)phenyl generates larger gaps than 1,3-di(2-pyridyl)-4,6-dimethylphenyl, while *ii* generates smaller gaps than *az*.

The bimetallic salt carrying the pincer ligand 1,3-di(2-pyridyl)-4,6-dimethylphenyl and the *az*-bridging group is a moderate red emitter in PMMA film ($\Phi_L \approx 0.50$). For its part, the molecular bimetallic compound bearing the same pincer ligand and the *ii*-bridging group is a weak dual emitter ($\Phi_L \approx 0.004$) in the solid state, with emission in the red and NIR regions. In the context of the emissive properties of the discovered species, it is worth highlighting the mononuclear intermediate [Pt{κ^3-*N,C,N*-[py-C_6HMe_2-py]}{κ^1-*N*-[H*az*]}]-BF_4, which is a green emitter that achieves quantum yields close to unity, at room temperature, when diluted in PMMA and 1,2-dichloroethane at low concentrations.

We can say that the pincer ligands indeed allow governing the metal−metal bond distances of d^8-platinum bimetallic complexes. However, its use involves replacing the double bridge, typical of bimetallic complexes with chelating ligands, with a monobridge. This structural change significantly increases the flexibility of the subunits around the bridge. For this reason, the bridging ligand achieves special relevance in order to control the photophysical properties of the emitters.

EXPERIMENTAL SECTION

General Information. All reactions were carried out with exclusion of air using Schlenk-tube techniques or in a drybox. Instrumental methods and X-ray diffractometry analysis details are given in the Supporting Information. In the NMR spectra (Figures S1−S20) the chemical shifts (in ppm) are referenced to residual solvent peaks (^{1}H, $^{13}C\{^1H\}$), or external Na_2PtCl_6 ($^{195}Pt\{^1H\}$), while coupling constants are given in hertz. In the $^{13}C\{^1H\}$ NMR spectra not all $^{13}C-^{195}Pt$ couplings could be resolved and the signal assignment was performed based on their two-dimensional NMR spectra (HSQC and HMBC). Indolo[2,3-*b*]indole,[25] PtCl{κ^3-*N,C,N*-[py-C_6HMe_2-py]} (**1**),[17j] PtCl-{κ^3-*N,C,N*-[py-O-C_6H_3-O-py]}) (**2**),[17h] Pt(OH){κ^3-*N,C,N*-[py-C_6HMe_2-py]} (**3**),[18] and Pt(OH){κ^3-*N,C,N*-[py-O-C_6H_3-O-py]} (**4**)[18] were prepared according to the reported procedures.

Preparation of [Pt{κ^3-*N,C,N*-[py-C_6HMe_2-py]}{κ^1-*N*-[H*az*]}]BF_4 (5). A suspension of **1** (200 mg, 0.41 mmol) in acetone (10 mL) was treated with Ag[BF_4] (80 mg, 0.41 mmol) and the resulting mixture was stirred protected from the light for 2.5 h at room temperature. After this time, 7-azaindole (48 mg, 0.41 mmol) was added, the resulting suspension was filtered through Celite to remove the silver salts and the solvent was evaporated to ca. 0.5 mL. Addition of diethyl ether afforded a pale-yellow solid that was washed with diethyl ether (3 × 5 mL) and dried under vacuo. Yield: 257 mg (95%). Anal. Calcd for $C_{25}H_{21}BF_4N_4Pt$ (%): C, 45.54; H, 3.21; N, 8.50. Found: C, 45.43; H, 3.15; N, 8.42. HRMS (electrospray, *m*/*z*) calcd. for $C_{25}H_{21}N_4Pt$ $[M]^+$: 572.1411; found: 572.1407. IR (cm^{-1}): IR (cm^{-1}): ν(N−H) 3332, ν(C = N), ν(C = C), 1590 (w), 1563 (m), $\nu(BF_4)$ 1050−999 (vs). ^{1}H NMR (400.1 MHz, CD_2Cl_2, 298 K): δ 9.89 (s, 1H, NH), 8.59 (dd with ^{195}Pt satellites, J_{H-H} = 5.4, J_{H-H} = 1.0, J_{H-Pt} = 19.2, 1H, az), 8.39 (dd, J_{H-H} = 7.8, J_{H-H} = 0.8, 1H, az), 8.04−7.98 (4H py NCN), 7.59−7.48 (4H, 2H py NCN + 2H az), 7.09−7.03 (m, 2H, py NCN), 6.98 (s, 1H, Ph), 6.81−6.78 (m, 1H, az), 2.71 (s, 6H, CH_3). The high instability in solution of the complex prevented getting its $^{13}C\{^1H\}$ NMR spectrum at 298 K. For this reason, this spectrum was recorded at 223 K. $^{13}C\{^1H\}$-APT NMR (100.63 MHz, CD_2Cl_2, 223 K): δ 167.8 (s, C py NCN), 161.5 (s, C−Pt), 150.2 (s, CH py NCN), 146.2 (s, C az), 142.7 (s, CH az), 140.4 (s, CH py NCN), 138.0 (s, C Ph), 137.5 (s, C Ph), 132.9 (s, CH Ph), 132.2 (s, CH az), 127.6 (s, CH az), 123.6 (s, CH py NCN), 123.2 (s, CH py NCN), 117.9 (s, CH az), 102.5 (s, CH az), 22.0 (s, CH_3). $^{195}Pt\{^1H\}$ NMR (85.6 MHz, CD_2Cl_2, 298 K): δ −3755 (s).

Preparation of [Pt{κ^3-*N,C,N*-[py-C_6HMe_2-py]}{κ^1-*N*-[H*az*]}]-SbF_6 (5′). A suspension of **1** (100 mg, 0.204 mmol) in acetone (10 mL) was treated with Ag[SbF_6] (70 mg, 0.204 mmol) and the resulting mixture was stirred protected from the light for 2.5 h at room temperature. After this time, 7-azaindole (24 mg, 0.204 mmol) was added, the resulting suspension was filtered through Celite to remove the silver salts and the solvent was evaporated to ca. 0.5 mL. Addition of diethyl ether afforded a pale-yellow solid that was washed with diethyl ether (3 × 5 mL) and dried under vacuo. Yield: 157 mg (95%). Crystals suitable for X-ray diffraction analysis were obtained at 4 °C by vapor diffusion of diethyl ether into an acetone solution of the complex. Anal. Calcd for $C_{25}H_{21}F_6N_4PtSb$ (%): C, 37.15; H, 2.62; N, 6.93. Found: C, 37.11; H, 2.59; N, 6.86. IR (cm^{-1}): ν(N−H) 3372, ν(C = N), ν(C = C), 1592 (w), 1565 (m), $\nu(SbF_6)$ 654−641 (vs). ^{1}H NMR (400.1 MHz, CD_2Cl_2, 298 K): δ 9.51 (s, 1H, NH), 8.61 (dd with ^{195}Pt satellites, J_{H-H} = 5.6, J_{H-H} = 1.2, J_{H-Pt} = 19.8, 1H, az), 8.42 (d, J_{H-H} = 8.0, 1H, az), 8.05−7.98 (4H py NCN), 7.59−7.45 (4H, 2H py NCN + 2H az), 7.10−7.04 (m, 2H, py NCN), 7.01 (s, 1H, Ph), 6.85−6.80 (m, 1H, az), 2.72 (s, 6H, CH_3). $^{195}Pt\{^1H\}$ NMR (85.6 MHz, CD_2Cl_2, 298 K): δ −3761 (s).

Preparation of [Pt{κ^3-*N,C,N*-[py-O-C_6H_3-O-py]}{κ^1-*N*-[H*az*]}]-BF_4 (6). A suspension of **2** (200 mg, 0.405 mmol) in acetone (10 mL) was treated with Ag[BF_4] (79 mg, 0.405 mmol) and the resulting mixture was stirred protected from the light for 2.5 h at room temperature. After this time, 7-azaindole (48 mg, 0.405 mmol) was added, the resulting suspension was filtered through Celite to remove the silver salts and the solvent was evaporated to ca. 0.5 mL. Addition of diethyl ether afforded a white solid that was washed with diethyl ether (3 × 5 mL) and dried under vacuo. Yield: 254 mg (95%). Anal. Calcd for $C_{23}H_{17}BF_4N_4O_2Pt$ (%): C, 41.65; H, 2.58; N, 8.45. Found: C, 41.33; H, 2.27; N, 8.63. HRMS (electrospray, *m*/*z*) calcd. for $C_{23}H_{17}N_4O_2Pt$ $[M]^+$: 576.0996; found: 576.1020. IR (cm^{-1}): ν(N−H) 3303, ν(C = N), ν(C = C) 1614, 1593 (w), $\nu(BF_4)$ 1055−986 (vs). ^{1}H NMR (400.1 MHz, CD_2Cl_2, 298 K): δ 10.27 (s, 1H NH), 8.36 (dd, J_{H-H} = 5.6, J_{H-H} = 1.0, 1H az), 8.33 (d, J_{H-H} = 7.9, 1H az), 7.96−7.90 (m, 2H py NCN), 7.55 (t, J_{H-H} = 3.1, 1H az), 7.47 (d with ^{195}Pt satellites, J_{H-H} = 8.4, J_{H-Pt} = 30.0, 2H py NCN), 7.39−7.29 (3H, 1H az +2H py NCN), 7.25−7.20 (m, 1H Ph), 7.13 (d, J_{H-H} = 7.6, 2H Ph), 6.74−6.69 (3H, 2H py NCN + 1H az). $^{13}C\{^1H\}$-APT NMR (100.63 MHz, CD_2Cl_2, 298 K): δ 160.2 (s, C py NCN), 153.5 (s, C−Pt), 149.2 (s, CH py NCN), 146.3 (s, C az), 142.7 (s, CH az), 142.6 (s, CH py NCN), 133.1 (s, CH az), 129.4 (s, CH az), 127.4 (s, CH Ph), 125.2 (s, C az), 120.9 (s, CH py NCN), 118.4 (s, CH az), 117.4 (s, CH py NCN), 113.7 (s, CH Ph), 102.8 (s, CH az), 100.8 (s, C Ph). $^{195}Pt\{^1H\}$ NMR (85.6 MHz, CD_2Cl_2, 298 K): δ −3344 (s).

Preparation of Pt{κ^1-*N*-[H*ii*]}{κ^3-*N,C,N*-[py-C_6HMe_2-py]} (7). Indolo[2,3-*b*]indole (66 mg, 0.318 mmol) was added to a suspension of **3** (100 mg, 0.212 mmol) in acetone (5 mL), and the resulting mixture was stirred for 6 h at room temperature getting a reddish orange suspension. The solution was removed, and the orange solid was washed with diethyl ether (5 × 3 mL) and dried under vacuum. Yield:

https://doi.org/10.1021/acs.inorgchem.4c01712
Inorg. Chem. 2024, 63, 14482−14494

70 mg (50%). Crystals suitable for X-ray diffraction analysis were obtained at 4 °C by vapor diffusion of pentane into a dichloromethane solution of the complex. Anal. Calcd for $C_{32}H_{24}N_4Pt$ (%): C, 58.27; H, 3.67; N, 8.49. Found: C, 57.91; H, 3.43; N, 8.33. HRMS (electrospray, m/z) calcd. for $C_{32}H_{25}N_4Pt$ $[M + H]^+$: 660.1722; found: 660.1706. IR (cm^{-1}): ν(N−H) 3425 (w), ν(C = N), ν(C = C) 1603 (m), 1562 (w). ^1H NMR (400.1 MHz, CD_2Cl_2, 243 K): δ 8.16 (broad s, 1H NH), 7.99 (dd with ^{195}Pt satellites, J_{H-H} = 5.5, J_{H-H} = 1.1, J_{H-Pt} = 39.8, 2H py NCN), 7.93−7.82 (5H, 4H py NCN + 1H (ii), 7.79 (d, J_{H-H} = 7.2, 1H (ii), 7.62 (d, J_{H-H} = 7.6, 1H (ii), 7.23 (d, J_{H-H} = 7.8, 1H (ii), 7.12 (td, J_{H-H} = 7.5, J_{H-H} = 1.0, 1H (ii), 7.02 (td, J_{H-H} = 7.1, J_{H-H} = 1.2, 1H (ii), 6.98−6.91 (m, 2H (ii), 6.90−6.85 (3H, 2H py NCN + 1H Ph NCN), 2.68 (s, 6H CH_3). $^{13}C\{^1H\}$ NMR (100.63 MHz, CD_2Cl_2, 298 K): δ 169.6 (s, C py NCN), 169.1 (s, C−Pt), 155.8 (s, C (ii), 152.4 (s, CH py NCN), 149.0 (s, C (ii), 139.5 (s, CH py NCN), 139.3 (s, C Ph NCN), 139.2 (s, C (ii), 137.4 (s, C Ph NCN), 131.8 (s, CH Ph NCN), 125.2, 124.7 (both s, C (ii), 123.2 (s, CH py NCN), 123.1 (s, CH py NCN), 119.7, 118.0, 117.5, 117.4, 117.1, 117.0, 114.7, 110.7 (all s, CH (ii), 101.3 (s, C (ii), 22.1 (s, CH_3). $^{195}Pt\{^1H\}$ NMR (85.6 MHz, CD_2Cl_2, 298 K): δ −3558 (s).

Preparation of Pt{κ^1-*N*-[H*ii*]}{κ^3-*N,C,N*-[py−O−C_6H_3−O−py]} (8). Indolo[2,3-*b*]indole (66 mg, 0.316 mmol) was added to a suspension of **4** (100 mg, 0.210 mmol) in acetone (5 mL), and the resulting mixture was stirred for 6 h at room temperature getting a yellow solution. The solvent was removed under vacuum. The resulting yellow solid was purified by column chromatography in deactivated silica eluting with toluene. The eluted solution was evaporated to dryness, affording a yellow residue. Addition of pentane afforded a pale yellow solid, that was washed with pentane (3 × 5 mL) and dried under vacuum. Yield: 84 mg (60%). Anal. Calcd for $C_{30}H_{20}N_4O_2Pt$ (%): C, 54.30; H, 3.04; N, 8.44. Found: C, 54.25; H, 3.01; N, 8.36. HRMS (electrospray, m/z) calcd. for $C_{30}H_{20}N_4O_2Pt$ $[M]^+$: 663.1229; found: 663.1222. IR (cm^{-1}): ν(N−H) 3352 (w), ν(C = N), ν(C = C) 1609 (m), 1565 (w). ^1H NMR (400.1 MHz, CD_2Cl_2, 298 K): δ 7.94 (broad s, 1H NH), 7.86 (d, J_{H-H} = 7.6, 1H (ii), 7.82−7.71 (5H, 4H py NCN + 1H (ii), 7.51 (d, J_{H-H} = 7.9, 1H (ii), 7.38−7.29 (m, 2H py NCN), 7.23−7.17 (2H, 1H Ph NCN + 1H (ii), 7.15−7.08 (3H, 2H Ph NCN + 1H (ii), 7.02 (ddd, J_{H-H} = 7.2, J_{H-H} = 1.1, 1H (ii), 6.96 (ddd, J_{H-H} = 7.5, J_{H-H} = 1.2, 1H (ii), 6.89 (ddd, J_{H-H} = 7.5, J_{H-H} = 1.3, 1H (ii), 6.57−6.51 (m, 2H py NCN). $^{13}C\{^1H\}$ NMR (100.63 MHz, CD_2Cl_2, 298 K): δ 159.7 (s, C py NCN), 154.1 (s, C−Pt), 153.9 (s, C (ii), 151.5 (s, CH py NCN), 146.9 (s, C (ii), 141.6 (s, CH py NCN), 139.1 (s, C (ii), 126.1 (s, CH Ph NCN), 125.2, 124.4 (both s, C (ii), 120.2 (s, CH py NCN), 119.7, 118.3, 117.8, 117.6, 117.5, 117.3 (all s, CH (ii), 116.0 (s, CH py NCN), 114.3 (s, CH (ii), 113.1 (s, CH Ph NCN), 110.8 (s, CH (ii), 107.2 (s, C Ph NCN), 101.7 (s, C (ii). $^{195}Pt\{^1H\}$ NMR (85.6 MHz, CD_2Cl_2, 298 K): δ −3175 (s).

Preparation of [{Pt[κ^3-*N,C,N*-(py-C_6HMe_2-py)]}$_2$]{μ-*N,N*-[*az*]}BF_4 (9). Complex **3** (86 mg, 0.18 mmol) was added to a suspension of **5** (120 mg, 0.18 mmol) in acetone (5 mL), and the resulting suspension was stirred at room temperature for 24 h. After this time the solvent was removed and the resulting red solid was washed with cold acetone (2 × 3 mL), diethyl ether (3 × 5 mL), and dried under vacuum. Yield 139 mg (68%). Crystals suitable for X-ray diffraction analysis were obtained at 4 °C by vapor diffusion of diethyl ether into a dichloromethane solution of the complex. Anal. Calcd for $C_{43}H_{35}BF_4N_6Pt_2$: C, 46.41; H, 3.17; N, 7.55. Found: C, 46.15; H, 2.99; N, 7.52. HRMS (electrospray, m/z) calcd. for $C_{43}H_{35}N_6Pt_2$ $[M]^+$: 1025.2209; found: 1025.2202. IR (cm^{-1}): ν(C = N), ν(C = C) 1604 (w), 1548 (m), ν(BF_4) 1051−1031 (vs).^1H NMR (400.1 MHz, CD_2Cl_2, 298 K): δ 8.44−8.35 (m, 2H az), 7.80 (d, $^3J_{H-H}$ = 2.8, 1H az), 7.70−7.60 (m, 4H py NCN), 7.41 (t, $^3J_{H-H}$= 8.3, 4H py NCN), 7.28 (d with ^{195}Pt satellites, $^3J_{H-H}$ = 5.6, $^3J_{H-Pt}$ = 42.4, 4H py NCN), 7.20 (dd, $^3J_{H-H}$ = 7.70, $^3J_{H-H}$= 5.3, 1H az), 6.91 (d, $^3J_{H-H}$ = 2.8, 1H az), 6.60 (s, 2H Ph) 6.59−6.51 (m, 4H py NCN), 2.41 (s, 6H, CH_3), 2.41 (s, 6H, CH_3). $^{13}C\{^1H\}$ NMR (100.63 MHz, CD_2Cl_2, 298 K): δ 168.5, 168.1 (both s, C py NCN), 167.6, 165.2 (both s, C−Pt), 155.6 (s, C az), 150.7, 150.2 (both s, CH py NCN), 141.3, 140.6 (both s, CH az), 139.3, 139.0 (both s, CH py NCN), 137.8, 137.5, 136.8, 136.7 (all s, C Ph), 132.2, 131.9 (s, CH Ph), 130.5 (s, CH az), 127.3 (s, C az), 123.2 (s, CH py NCN), 122.9 (s, CH py NCN), 122.5 (s, CH py NCN), 122.3 (s, CH py NCN), 114.6, 101.9 (both s, CH az), 22.2, 22.1 (both s, CH_3). $^{195}Pt\{^1H\}$ NMR (85.6 MHz, CD_2Cl_2, 298 K): δ −3462, −3563.

[{Pt[κ^3-*N,C,N*-(py-O-C_6H_3-O-py)]}$_2$]{μ-*N,N*-[*az*]}BF_4 (10). Complex **4** (86 mg, 0.18 mmol) was added to a suspension of **6** (120 mg, 0.18 mmol) in acetone (5 mL), and the resulting suspension was stirred at room temperature for 24 h. After this time the supernatant solution was removed and the yellowish white solid was washed with cold acetone (2 × 2 mL), diethyl ether (3 × 5 mL) and dried under vacuum. Yield 131 mg (65%). Crystals suitable for X-ray diffraction analysis were obtained at 4 °C by vapor diffusion of diethyl ether into a dichloromethane solution of the complex. Anal. Calcd for $C_{39}H_{27}BF_4N_6O_4Pt_2$: C, 41.80; H, 2.43; N, 7.50. Found: C, 41.46; H, 2.67; N, 7.77. HRMS (electrospray, m/z) calcd.for $C_{39}H_{27}N_6O_4Pt_2$ $[M]^+$: 1033.1384; found: 1033.1413. IR (cm^{-1}): ν(C = N), ν(C = C), 1614 (m), 1568 (w), ν(BF_4) 1053 (vs). ^1H NMR (400.1 MHz, CD_2Cl_2, 298 K): δ 8.47 (dd, J_{H-H} = 5.4, J_{H-H} = 1.6, 1H az), 8.31 (dd, J_{H-H} = 7.9, J_{H-H} = 1.3, 1H az), 7.75 (d, J_{H-H} = 3.1, 1H az), 7.60−7.50 (4H py NCN), 7.32−7.00 (5H, 1H az +4H py NCN), 6.96−6.92 (3H, 1H az +2H Ph), 6.85 (t, J_{H-H} = 8.8, 4H py NCN), 6.66 (d, J_{H-H} = 8.0, 4H Ph), 6.42−6.32 (4H py NCN). $^{13}C\{^1H\}$-APT NMR (100.63 MHz, CD_2Cl_2, 298 K): δ 159.1, 158.9 (both s, C py NCN), 153.0 (s, C−Pt), 152.9 (s, C az), 152.7 (s, C−Pt), 149.4, 148.5 (both s, CH py NCN), 142.3 (s, CH az), 141.9, 141.6 (both s, CH py NCN), 139.9 (s, CH az), 131.6 (s, CH az), 128.1 (s, C az), 126.5, 126.1 (both s, CH Ph), 120.0, 119.6 (both s, CH py NCN), 116.4, (s, CH py NCN), 116.1 (s, CH az), 112.9, 112.6 (both s, CH Ph), 104.5 (s, CH az), 101.8, 99.4 (both s, C Ph). $^{195}Pt\{^1H\}$ NMR (85.6 MHz, CD_2Cl_2, 298 K): δ −3061, −3152.

Preparation of {Pt[κ^3-*N,C,N*-(py-C_6HMe_2-py)]}$_2$]{μ-*N,N*-[*ii*]} (11). Complex **3** (80 mg, 0.17 mmol) was added to a suspension of **7** (112 mg, 0.17 mmol) in acetone (5 mL), and the resulting suspension was stirred at room temperature for 24 h. After this time the solvent was removed and the resulting deep red solid was washed with acetone (3 × 5 mL), dichloromethane (3 × 5 mL), pentane (3 × 5 mL) and dried under vacuum. Yield 164 mg (87%). Crystals suitable for X-ray diffraction analysis were obtained as follows: Acetone (10 mL) was layered over a solution of **3** (50 mg, 0.106 mmol) in acetone (50 mL) placed in a Schlenk flask, and then, a solution of indolo[2,3-*b*]indole (11 mg, 0.053 mmol) in acetone (10 mL) was added slowly over the acetone layer. After 24 h standing at room temperature deep red crystals were collected. Anal. Calcd for $C_{50}H_{38}N_6Pt_2$ (%): C, 53.95; H, 3.44; N, 7.55. Found: C, 53.81; H, 3.39; N, 7.47. IR (cm^{-1}): ν(C═N), ν(C═C) 1595 (m), 1546 (w). The high insolubility of the complex prevented getting its mass and NMR spectra.

■ ASSOCIATED CONTENT

Supporting Information

The Supporting Information is available free of charge at https://pubs.acs.org/doi/10.1021/acs.inorgchem.4c01712.

General information for the experimental section, NMR spectra, structural analysis of complexes **5**, **7**, **9**, **10**, and **11**, computational details, energies of optimized structures, observed and calculated UV−vis spectra of complexes **5**−**11**, analysis of computed UV/vis data, theoretical analysis of molecular orbitals, cyclic voltammograms of complexes **5**−**10**, and photophysical studies (PDF)

Atomic coordinates of optimized complexes (XYZ)

Accession Codes

CCDC 2348930−2348934 contain the supplementary crystallographic data for this paper. These data can be obtained free of charge via www.ccdc.cam.ac.uk/data_request/cif., or by emailing data_request@ccdc.cam.ac.uk, or by contacting The Cambridge Crystallographic Data Centre, 12 Union Road, Cambridge CB2 1EZ, UK; fax: +44 1223 336 033.

https://doi.org/10.1021/acs.inorgchem.4c01712
Inorg. Chem. 2024, 63, 14482−14494

AUTHOR INFORMATION

Corresponding Author

Miguel A. Esteruelas − *Departamento de Química Inorgánica - Instituto de Síntesis Química y Catálisis Homogénea (ISQCH) - Centro de Innovación en Química Avanzada (ORFEO−CINQA), Universidad de Zaragoza - CSIC, Zaragoza 50009, Spain;* orcid.org/0000-0002-4829-7590; Email: maester@unizar.es

Authors

Sonia Moreno-Blázquez − *Departamento de Química Inorgánica - Instituto de Síntesis Química y Catálisis Homogénea (ISQCH) - Centro de Innovación en Química Avanzada (ORFEO−CINQA), Universidad de Zaragoza - CSIC, Zaragoza 50009, Spain*

Montserrat Oliván − *Departamento de Química Inorgánica - Instituto de Síntesis Química y Catálisis Homogénea (ISQCH) - Centro de Innovación en Química Avanzada (ORFEO−CINQA), Universidad de Zaragoza - CSIC, Zaragoza 50009, Spain;* orcid.org/0000-0003-0381-0917

Enrique Oñate − *Departamento de Química Inorgánica - Instituto de Síntesis Química y Catálisis Homogénea (ISQCH) - Centro de Innovación en Química Avanzada (ORFEO−CINQA), Universidad de Zaragoza - CSIC, Zaragoza 50009, Spain;* orcid.org/0000-0003-2094-719X

Complete contact information is available at: https://pubs.acs.org/10.1021/acs.inorgchem.4c01712

Notes

The authors declare no competing financial interest.

ACKNOWLEDGMENTS

Financial support from the MICIN/AEI/10.13039/501100011033 (PID2020-115286GB-I00 and RED2022-134287-T), Gobierno de Aragón (E06_23R), FEDER, and the European Social Fund.

REFERENCES

(1) (a) Yoshida, M.; Kato, M. Regulation of metal−metal interactions and chromic phenomena of multi-decker platinum complexes having π-systems. *Coord. Chem. Rev.* **2018**, *355*, 101−115. (b) Puttock, E. V.; Walden, M. T.; Williams, J. A. G. The luminescence properties of multinuclear platinum complexes. *Coord. Chem. Rev.* **2018**, *367*, 127−162. (c) Chaaban, M.; Zhou, C.; Lin, H.; Chyi, B.; Ma, B. Platinum(II) binuclear complexes: Molecular structures, photophysical properties, and applications. *J. Mater. Chem. C* **2019**, *7*, 5910−5924. (d) Horiuchi, S.; Umakoshi, K. Recent advances in pyrazolato-bridged homo- and heterometallic polynuclear platinum and palladium complexes. *Coord. Chem. Rev.* **2023**, *476*, 214924.

(2) Chaaban, M.; Chi, Y.-C.; Worku, M.; Zhou, C.; Lin, H.; Lee, S.; Ben-Akacha, A.; Lin, X.; Huang, C.; Ma, B. Thiazol-2-thiolate-Bridged Binuclear Platinum(II) Complexes with High Photoluminescence Quantum Efficiencies of up to Near Unity. *Inorg. Chem.* **2020**, *59*, 13109−13116.

(3) Roy, S.; Lopez, A. A.; Yarnell, J. E.; Castellano, F. N. Metal−Metal-to-Ligand Charge Transfer in Pt(II) Dimers Bridged by Pyridyl and Quinoline Thiols. *Inorg. Chem.* **2022**, *61*, 121−130.

(4) (a) Mills, A. W.; Valentine, A. J. S.; Hoang, K.; Roy, S.; Castellano, F. N.; Chen, L. X.; Li, X. General Design Rules for Bimetallic Platinum(II) Complexes. *J. Phys. Chem. A* **2021**, *125*, 9438−9449. (b) Kromer, S.; Roy, S.; Yarnell, J. E.; Taliaferro, C. M.; Castellano, F. N. Excited state processes of dinuclear Pt(II) complexes bridged by 8-hydroxyquinoline. *Dalton Trans.* **2023**, *52*, 4008−4016.

(5) (a) Chakraborty, A.; Yarnell, J. E.; Sommer, R. D.; Roy, S.; Castellano, F. N. Excited-State Processes of Cyclometalated Platinum-(II) Charge-Transfer Dimers Bridged by Hydroxypyridines. *Inorg. Chem.* **2018**, *57*, 1298−1310. (b) Leshchev, D.; Valentine, A. J. S.; Kim, P.; Mills, A. W.; Roy, S.; Chakraborty, A.; Biasin, E.; Haldrup, K.; Hsu, D. J.; Kirschner, M. S.; et al. Revealing Excited-State Trajectories on Potential Energy Surfaces with Atomic Resolution in Real Time. *Angew. Chem., Int. Ed.* **2023**, *62*, No. e202304615.

(6) (a) Chakraborty, A.; Deaton, J. C.; Haefele, A.; Castellano, F. N. Charge-Transfer and Ligand-Localized Photophysics in Luminescent Cyclometalated Pyrazolate-Bridged Dinuclear Platinum(II) Complexes. *Organometallics* **2013**, *32*, 3819−3829. (b) McCusker, C. E.; Chakraborty, A.; Castellano, F. N. Excited State Equilibrium Induced Lifetime Extension in a Dinuclear Platinum(II) complex. *J. Phys. Chem. A* **2014**, *118*, 10391−10399. (c) Zhou, C.; Tian, Y.; Yuan, Z.; Han, M.; Wang, J.; Zhu, L.; Tameh, M. S.; Huang, C.; Ma, B. Precise Design of Phosphorescent Molecular Butterflies with Tunable Photoinduced Structural Change and dual Emission. *Angew. Chem., Int. Ed.* **2015**, *54*, 9591−9595. (d) Brown-Xu, S. E.; Kelley, M. S. J.; Fransted, K. A.; Chakraborty, A.; Schatz, G. C.; Castellano, F. N.; Chen, L. X. Tunable Excited-State Properties and Dynamics as a Function of Pt-Pt Distance in Pyrazolate-Bridged Pt(II) Dimers. *J. Phys. Chem. A* **2016**, *120*, 543−550. (e) Kim, P.; Kelley, M. S.; Chakraborty, A.; Wong, N. L.; Van Duyne, R. P.; Schatz, G. C.; Castellano, F. N.; Chen, L. X. Coherent Vibrational Wavepacket Dynamics in Platinum(II) Dimers and Their Implications. *J. Phys. Chem. C* **2018**, *122*, 14195−14204. (f) Weingartz, N. P.; Mara, M. W.; Roy, S.; Hong, J.; Chakraborty, A.; Brown-Xu, S. E.; Phelan, B. T.; Castellano, F. N.; Chen, L. X. Excited-State Bond Contraction and Charge Migration in a Platinum Dimer Complex Characterized by X-ray and Optical Transient Absorption Spectroscopy. *J. Phys. Chem. A* **2021**, *125*, 8891−8898. (g) Kim, T. W.; Kim, P.; Mills, A. W.; Chakraborty, A.; Kromer, S.; Valentine, A. J. S.; Castellano, F. N.; Li, X.; Chen, L. X. Ligand-Structure-Dependent Coherent Vibrational Wavepacket Dynamics in Pyrazolate-Bridged Pt(II) Dimers. *J. Phys. Chem. C* **2022**, *126*, 11487−11497. (h) Gómez de Segura, D.; Corral-Zorzano, A.; Alcolea, E.; Moreno, M. T.; Lalinde, E. Phenylbenzothiazole-Based Platinum(II) and Diplatinum(II) and (III) Complexes with Pyrazolate Groups: Optical Properties and Photocatalysis. *Inorg. Chem.* **2024**, *63*, 1589−1606.

(7) Zhang, H.; Liu, C.; Zhang, J.; Du, C.-X.; Zhang, B. Highly Emissive Platinum(II) Complexes Bearing Bulky Phenyltriazolate Ligands: Synthesis, Structure, and Photophysics. *Organometallics* **2022**, *41*, 1381−1390.

(8) Lalinde, E.; Moreno, M. T.; Ruiz, S.; Sánchez, S. Synthesis, Structural, and Photophysical Studies of Phenylquinoline and Phenylquinolinyl Alkynyl Based Pt(II) Complexes. *Organometallics* **2014**, *33*, 3078−3090.

(9) (a) Pinter, P.; Soellner, J.; Strassner, T. Photophysical Properties of Phosphorescent Mono- and Bimetallic Platinum(II) Complexes with C^C* Cyclometalating NHC Ligands. *Organometallics* **2021**, *40*, 557−563. (b) Sicilia, V.; Arnal, L.; Escudero, D.; Fuertes, S.; Martin, A. Chameleonic Photo- and Mechanoluminescence in Pyrazolate-Bridged NHC Cyclometalated Platinum Complexes. *Inorg. Chem.* **2021**, *60*, 12274−12284. (c) Arnal, L.; Escudero, D.; Fuertes, S.; Martin, A.; Sicilia, V. High-Valent Pyrazolate-Bridged Platinum Complexes: A Joint Experimental and Theoretical Study. *Inorg. Chem.* **2022**, *61*, 12559−12569.

(10) (a) Pinter, P.; Soellner, J.; Strassner, T. Metallophilic Interactions in Bimetallic Cyclometalated Platinum(II) N-Heterocyclic Carbene Complexes. *Eur. J. Inorg. Chem.* **2021**, *2021*, 3104−3107. (b) Xue, M.; Lam, T.-L.; Cheng, G.; Liu, W.; Low, K.-H.; Du, L.; Xu, S.; Hung, F.-F.; Phillips, D. L.; Che, C.-M. Exceedingly Stable Luminescent Dinuclear Pt(II) Complexes with Ditopic Formamidinate Bridging Ligands for High-Performance Red and Deep-Red OLEDs with LT_{97} up to 2446 h at 1000 cd m^{-2}. *Adv. Opt. Mater.* **2022**, *10*, 2200741. (c) Stipurin, S.; Strassner, T. Phosphorescent Bimetallic C^C* Platinum(II) Complexes with Bridging Substituted Diphenylformamidinates. *Chem.-Eur. J.* **2022**, *28*, No. e202202227.

(11) Park, H. J.; Boelke, C. L.; Cheong, P. H.-Y.; Hwang, D.-H. Dinuclear Pt(II) Complexes with Red and NIR Emission Governed by Ligand Control of the Intramolecular Pt-Pt Distance. *Inorg. Chem.* **2022**, *61*, 5178−5183.
(12) (a) Freeman, G. R.; Williams, J. A. G. Metal Complexes of Pincer Ligands: Excited States, Photochemistry, and Luminescence. *Top. Organomet. Chem.* **2013**, *40*, 89−130. (b) Williams, J. A. G.; Wilkinson, A. J.; Whittle, V. L. Light-emitting iridium complexes with tridentate ligands. *Dalton Trans.* **2008**, 2081−2099. (c) Yam, V.-W.-W.; Au, V. K.-M.; Leung, S. Y.-L. Light-Emitting Self-Assembled Materials Based on d^8 and d^{10} Transition Metal Complexes. *Chem. Rev.* **2015**, *115*, 7589−7728. (d) Chi, Y.; Chang, T.-K.; Ganesan, P.; Rajakannu, P. Emissive bis-tridentate Ir(III) metal complexes: Tactics, photophysics and applications. *Coord. Chem. Rev.* **2017**, *346*, 91−100. (e) Chan, A. K.-W.; Yam, V.-W.-W. Precise Modulation of Molecular Building Blocks from Tweezers to Rectangles for Recognition and Stimuli-Responsive Processes. *Acc. Chem. Res.* **2018**, *51*, 3041−3051. (f) Haque, A.; Xu, L.; Al-Balushi, R. A.; Al-Suti, M. K.; Ilmi, R.; Guo, Z.; Khan, M. S.; Wong, W.-Y.; Raithby, P. R. Cyclometallated tridentate platinum(II) arylacetylide complexes: Old wine in new bottles. *Chem. Soc. Rev.* **2019**, *48*, 5547−5563. (g) Buil, M. L.; Esteruelas, M. A.; López, A. M. Recent Advances in Synthesis of Molecular Heteroleptic Osmium and Iridium Phosphorescent Emitters. *Eur. J. Inorg. Chem.* **2021**, *2021*, 4731−4761.
(13) (a) Bailey, J. A.; Gray, H. B. A μ-Pyrazolyl Terpyridineplatinum-(II) Dimer. *Acta Crystallogr.* **1992**, *C48*, 1420−1422. (b) Tzeng, B.-C.; Fu, W.-F.; Che, C.-M.; Chao, H.-Y.; Cheung, K.-K.; Peng, S.-M. Structures and photoluminescence of dinuclear platinum(II) and palladium(II) complexes with bridging thiolates and 2,2'-bipyridine or 2,2':6',2"-terpyridine ligands. *J. Chem. Soc., Dalton Trans.* **1999**, 1017−1023. (c) Lowe, G.; Ross, S. A.; Probert, M.; Cowley, A. The X-ray crystal structure of N,S-bis[(4'-chloro-2,2':6',2"-terpyridine) platinum-(II)]-2-mercaptoimidazole tris-hexafluorophosphate and tris-[(2,2':6',2"-terpyridine)platinum(II)]sulfonium tetra-perchlorate. *Chem. Commun.* **2001**, 1288−1289. (d) Wang, K.-W.; Chen, J.-L.; Cheng, Y.-M.; Chung, M.-W.; Hsieh, C.-C.; Lee, G.-H.; Chou, P.-T.; Chen, K.; Chi, Y. Mono- versus Dinuclear Pt(II) 6-(5-Trifluoromethyl-Pyrazol-3-yl)-2,2'-Bipyridine Complexes: Synthesis, Characterization, and Remarkable Difference in Luminescent Properties. *Inorg. Chem.* **2010**, *49*, 1372−1383. (e) Zhang, H.-X.; Kato, M.; Sasaki, Y.; Ohba, T.; Ito, H.; Kobayashi, A.; Chang, H.-C.; Uosaki, K. Terpyridine platinum(II) complexes containing triazine di- or tri-thiolate bridges: Structures, luminescence, electrochemistry, and aggregation. *Dalton Trans.* **2012**, *41*, 11497−11506. (f) Leung, S. Y.-L.; Tam, A.-Y.-Y.; Tao, C.-H.; Chow, H. S.; Yam, V.-W.-W. Single-Turn Helix-Coil Strands Stabilized by Metal···Metal and π-π Interactions of the Alkynylplatinum(II) Terpyridyl Moieties in *meta*-Phenylene Ethynylene Foldamers. *J. Am. Chem. Soc.* **2012**, *134*, 1047−1056. (g) Zhang, R.; Zhang, Z.; Liang, Z.; Han, Y.; Ai, X.; Cao, R. Syntheses and Structural Characterizations of Mononuclear and Dinuclear Platinum-(II) Terpyridyl Acetylide Complexes. *ChemistrySelect* **2017**, *2*, 5436−5443.
(14) (a) Lu, W.; Chan, M. C. W.; Zhu, N.; Che, C.-M.; Li, C.; Hui, Z. Structural and Spectroscopic Studies on Pt···Pt and π-π Interactions in Luminescent Multinuclear Cyclometalated Platinum(II) Homologues Tethered by Oligophosphine Auxiliaries. *J. Am. Chem. Soc.* **2004**, *126*, 7639−7651. (b) Kui, S. C. F.; Sham, I. H. T.; Cheung, C. C. C.; Ma, C.-W.; Yan, B.; Zhu, M.; Che, C.-M.; Fu, W.-F. Platinum(II) Complexes with π-Conjugated, Naphthyl-Substituted, Cyclometalated Ligands (RC^N^N): Structures and Photo- and Electroluminescence. *Chem.-Eur. J.* **2007**, *13*, 417−435. (c) Sun, R. W.-Y.; Chow, A. L.-F.; Li, X.-H.; Yan, J. J.; Chui, S. S.-Y.; Che, C.-M. Luminescent cyclometalated platinum(II) complexes containing *N*-heterocyclic carbene ligands with potent *in vitro* and *in vivo* anti-cancer properties accumulate in cytoplasmic structures of cancer cells. *Chem. Sci.* **2011**, *2*, 728−736. (d) Zhang, X.-P.; Wang, L.-L.; Qi, X.-W.; Zhang, D.-S.; Yang, Q.-Y.; Shi, Z.-F.; Lin, Q.; Wu, T. Pt···Pt interaction triggered tuning of circularly polarized luminescence activity in chiral dinuclear platinum(II) complexes. *Dalton Trans.* **2018**, *47*, 10179−10186. (e) Ho, Y.-M.; Au, N.-P. B.; Wong, K.-L.; Chan, C. T.-L.; Kwok, W.-M.; Law, G.-L.; Tang, K.-K.; Wong, W.-Y.; Ma, C.-H. E.; Lam, M. H.-W. A lysosome-specific two-photon phosphorescent binuclear cyclometalated platinum(II) probe for *in vivo* imaging of live neurons. *Chem. Commun.* **2014**, *50*, 4161−4163. (f) Wang, G.-X.; Feng, K.; Crossley, M. J.; Xing, L.-B.; Xiao, H.-Y.; Li, W.; Tung, C.-H.; Wu, L.-Z. Conformation-Controlled Diplatinum(II)−Ferrocene Dyads to Achieve Long-Lived Charge-Separated States. *Chem.-Eur. J.* **2016**, *22*, 11962−11966.
(15) (a) Lai, S.-W.; Lam, H.-W.; Lu, W.; Cheung, K.-K.; Che, C.-M. Observation of Low-Energy Metal−Metal-to-Ligand Charge Transfer Absorption and Emission: Electronic Spectroscopy of Cyclometalated Platinum(II) Complexes with Isocyanide Ligands. *Organometallics* **2002**, *21*, 226−234. (b) Wong, K. M.-C.; Zhu, N.; Yam, V.-W.-W. Unprecedented formation of an acetamidate-bridged dinuclear platinum(II) terpyridyl complex-correlation of luminescence properties with the crystal forms and dimerization studies in solution. *Chem. Commun.* **2006**, 3441−3443.
(16) (a) Williams, J. A. G. The coordination chemistry of dipyridylbenzene: N-deficient terpyridine or panacea for brightly luminescent metal complexes? *Chem. Soc. Rev.* **2009**, *38*, 1783−1801. (b) Valdés, H.; González-Sebastián, L.; Morales-Morales, D. Aromatic *para*-functionalized NCN pincer compounds. *J. Organomet. Chem.* **2017**, *845*, 229−257.
(17) (a) Cárdenas, D. J.; Echavarren, A. M.; Ramírez de Arellano, M. C. Divergent Behavior of Palladium(II) and Platinum(II) in the Metalation of 1,3-Di(2-pyridyl)benzene. *Organometallics* **1999**, *18*, 3337−3341. (b) Chiu, B. K.-W.; Lam, M. H.-W.; Lee, D. Y.-K.; Wong, W.-Y. Synthesis, characterization and spectroscopic studies of cyclometalated platinum(II) complexes containing meta-bis(2-pyridoxy)-benzene. *J. Organomet. Chem.* **2004**, *689*, 2888−2899. (c) Farley, S. J.; Rochester, D. L.; Thompson, A. L.; Howard, J. A. K.; Williams, J. A. G. Controlling Emission Energy, Self-Quenching, and Excimer Formation in Highly Luminescent N^C^N-Coordinated Platinum(II) Complexes. *Inorg. Chem.* **2005**, *44*, 9690−9703. (d) Chen, Y.; Li, K.; Lu, W.; Chui, S. S.-Y.; Ma, C.-W.; Che, C.-M. Photoresponsive Supramolecular Organometallic Nanosheets Induced by Pt^{II}···Pt^{II} and C−H···π Interactions. *Angew. Chem., Int. Ed.* **2009**, *48*, 9909−9913. (e) Koo, C.-K.; Wong, K.-L.; Lau, K.-C.; Wong, W.-Y.; Lam, M. H.-W. The Controlled Formation and Cleavage of an Intramolecular d^8−d^8 Pt−Pt Interaction in a Dinuclear Cycloplatinated Molecular "Pivot-Hinge. *Chem.-Eur. J.* **2009**, *15*, 7689−7697. (f) Chen, Y.; Lu, W.; Che, C.-M. Luminescent Pincer-Type Cyclometalated Platinum(II) Complexes with Auxiliary Isocyanide Ligands: Phase-Transfer Preparation, Solvatomorphism, and Self-Aggregation. *Organometallics* **2013**, *32*, 350−353. (g) Tarran, W. A.; Freeman, G. R.; Murphy, L.; Benham, A. M.; Kataky, R.; Williams, J. A. G. Platinum(II) Complexes of N^C^N-Coordinating 1,3-Bis(2-pyridyl)benzene Ligands: Thiolate Coligands Lead to Strong Red Luminescence from Charge-Transfer States. *Inorg. Chem.* **2014**, *53*, 5738−5749. (h) Kim, Y. T.; Yoon, M. S. Synthesis of a Platinum-Pincer Complex and Application to Catalytic Silylcyanation. *Appl. Chem. Eng.* **2016**, *27*, 366−370. (i) Gong, Z.-L.; Zhong, Y.-W.; Yao, J. Regulation of intra- and intermolecular Pt−Pt and π−π interactions of a U-shaped diplatinum complex to achieve pseudo-polymorphic emissions in solution and crystalline states. *J. Mater. Chem. C* **2017**, *5*, 7222−7229. (j) Schulze, B.; Friebe, C.; Jäger, M.; Görls, H.; Birckner, E.; Winter, A.; Schubert, U. S. Pt^{II} Phosphors with Click-Derived 1,2,3-Triazole-Containing Tridentate Chelates. *Organometallics* **2018**, *37*, 145−155. (k) Cinninger, L. M.; Bastatas, L. D.; Shen, Y.; Holliday, B. J.; Slinker, J. D. Luminescent properties of a 3,5-diphenylpyrazole bridged Pt(II) dimer. *Dalton Trans.* **2019**, *48*, 9684−9691. (l) Li, B.; Li, Y.; Chan, M. H.-Y.; Yam, V.-W.-W. Phosphorescent Cyclometalated Platinum(II) Enantiomers with Circularly Polarized Luminescence Properties and Their Assembly Behaviors. *J. Am. Chem. Soc.* **2021**, *143*, 21676−21684. (m) Poveda, D.; Vivancos, Á.; Bautista, D.; González-Herrero, P. Photochemically Induced Cyclometalations at Simple Platinum(II) Precursors. *Inorg. Chem.* **2023**, *62*, 6207−6213. (n) Lorenzo-Aparicio, C.; Moreno-Blázquez, S.; Oliván, M.; Esteruelas, M. A.; Gómez Gallego, M.; García-Álvarez, P.; Cabeza, J. A.; Sierra, M. A. Synthesis, Structure, and Photophysical Properties of Platinum(II)

https://doi.org/10.1021/acs.inorgchem.4c01712
Inorg. Chem. 2024, 63, 14482−14494

(N , C , N ′) Pincer Complexes Derived from Purine Nucleobases. *Inorg. Chem.* **2023**, *62*, 8232−8248.
(18) Esteruelas, M. A.; Moreno-Blázquez, S.; Oliván, M.; Oñate, E. Competition between N,C,N-Pincer and N,N-Chelate Ligands in Platinum(II). *Inorg. Chem.* **2023**, *62*, 10152−10170.
(19) (a) Bailey, J. A.; Miskowski, V. M.; Gray, H. B. Spectroscopic and Structural Properties of Binuclear Platinum-Terpyridine Complexes. *Inorg. Chem.* **1993**, *32*, 369−370. (b) Bailey, J. A.; Miskowski, V. M.; Gray, H. B. A diphenylformamidinate-bridged terpyridineplatinum(II) dimer. *Acta Crystallogr., Sect. C: Cryst. Struct. Commun.* **1993**, *49*, 793−796. (c) Casas, J. M.; Diosdado, B. E.; Forniés, J.; Martín, A.; Rueda, A. J.; Orpen, A. G. Synthesis of Binuclear Platinum Complexes Containing the Ligands 8-Naphthyridine, 2-Aminopyridine, and 7-Azaindolate. An Experimental Study of the Steric Hindrance of the Bulky Pentafluorophenyl Ligands in the Synthesis of Binuclear Complexes. *Inorg. Chem.* **2008**, *47*, 8767−8775. (d) Ruiz, J.; Rodríguez, V.; de Haro, C.; Espinosa, A.; Pérez, J.; Janiak, C. New 7-azaindole palladium and platinum complexes: Crystal structures and theoretical calculations. *In vitro* anticancer activity of the platinum compounds. *Dalton Trans.* **2010**, *39*, 3290−3301.
(20) The replacement of $[BF_4]^-$ by $[SbF_6]^-$ was necessary to obtain crystals suitable for X-ray diffraction analysis. The $[SbF_6]^-$-salt was prepared in a similar way to the $[BF_4]^-$-salt, using $Ag[SbF_6]$ instead of $Ag[BF_4]$ as a dehalogenation agent.
(21) (a) Hunter, C. A.; Sanders, J. K. M. The Nature of π - π Interactions. *J. Am. Chem. Soc.* **1990**, *112*, 5525−5534. (b) Janiak, C. A critical account on π - π stacking in metal complexes with aromatic nitrogen-containing ligands. *J. Chem. Soc., Dalton Trans.* **2000**, 3885−3896. (c) Martinez, C. R.; Iverson, B. L. Rethinking the term "pi-stacking. *Chem. Sci.* **2012**, *3*, 2191−2201. (d) Trujillo, C.; Sánchez-Sanz, G. A Study of π-π Stacking Interactions and Aromaticity in Polycyclic Aromatic Hydrocarbon/Nucleobase Complexes. *ChemPhysChem* **2016**, *17*, 395−405.
(22) Lorenzo-Aparicio, C.; García-Álvarez, P.; Cabeza, J. A.; Gómez-Gallego, M.; Sierra, M. A. Nucleobase Stacking Sustained by Pt−Pt Interactions. *ChemistryEurope* **2024**, *2*, No. e202300065. and references therein.
(23) (a) Pettijohn, C. N.; Jochnowitz, E. B.; Chuong, B.; Nagle, J. K.; Vogler, A. Luminescent excimers and exciplexes of Pt^{II} compounds. *Coord. Chem. Rev.* **1998**, *171*, 85−92. (b) Tears, D. K. C.; McMillin, D. R. Exciplex quenching of photoexcited platinum(II) terpyridines: Influence of the orbital parentage. *Coord. Chem. Rev.* **2001**, *211*, 195−205. (c) Mróz, W.; Botta, C.; Giovanella, U.; Rossi, E.; Colombo, A.; Dragonetti, C.; Roberto, D.; Ugo, R.; Valore, A.; Williams, J. A. G. Cyclometallated platinum(II) complexes of 1,3-di(2-pyridyl)benzenes for solution-processable WOLEDs exploiting monomer and excimer phosphorescence. *J. Mater. Chem.* **2011**, *21*, 8653−8661. (d) Stengel, I.; Strassert, C. A.; Plummer, E. A.; Chien, C.-H.; De Cola, L.; Bäuerle, P. Postfuncionalization of Luminescent Bipyridine Pt^{II} Bisacetylides by Click Chemistry. *Eur. J. Inorg. Chem.* **2012**, *2012*, 1795−1809. (e) Rossi, E.; Colombo, A.; Dragonetti, C.; Roberto, D.; Ugo, R.; Valore, A.; Falciola, L.; Brulatti, P.; Cocchi, M.; Williams, J. A. G. Novel N^C^N-cyclometallated platinum complexes with acetylide co-ligands as efficient phosphors for OLEDs. *J. Mater. Chem.* **2012**, *22*, 10650−10655. (f) Li, K.; Zou, T.; Chen, Y.; Guan, X.; Che, C.-M. Pincer-Type Platinum(II) Complexes Containing N-Heterocyclic Carbene (NHC) Ligand: Structures, Photophysical and Anion-Binding Properties, and Anticancer Activities. *Chem.-Eur. J.* **2015**, *21*, 7441−7453. (g) Stegemann, L.; Sanning, J.; Daniliuc, C. G.; Strassert, C. A. Influence of the monodentate ancillary ligand on the photophysical properties of Pt(II) complexes bearing a symmetric dianionic tridentate luminophore. *J. Nat. Res. B* **2016**, *71*, 1087−1093. (h) Hebenbrock, M.; Stegemann, L.; Kösters, J.; Doltsinis, N. L.; Müller, J.; Strassert, C. A. Phosphorescent Pt(II) complexes bearing a monoanionic C^N^N luminophore and tunable ancillary ligands. *Dalton Trans.* **2017**, *46*, 3160−3169. (i) Yang, X.; Guo, H.; Xu, X.; Sun, Y.; Zhou, G.; Ma, W.; Wu, Z. Enhancing Molecular Aggregations by Intermolecular Hydrogen Bonds to Develop Phosphorescent Emitters for High-Performance Near-Infrared OLEDs. *Adv. Sci.* **2019**, *6*, 1801930. (j) Sun, Y.; Yang, X.; Liu, B.; Guo, H.; Zhou, G.; Ma, W.; Wu, Z. Aggregation-induced emission triggered by the radiative-transition-switch of a cyclometallated Pt(II) complex. *J. Mater. Chem. C* **2019**, *7*, 12552−12559. (k) Martínez-Junquera, M.; Lara, R.; Lalinde, E.; Moreno, M. T. Isomerism, aggregation-induced emission and mechanochromism of isocyanide cycloplatinated(II) complexes. *J. Mater. Chem. C* **2020**, *8*, 7221−7233. (l) Hruzd, M.; le Poul, N.; Cordier, M.; Kahlal, S.; Saillard, J.-Y.; Achelle, S.; Gauthier, S. Luminescent cyclometalated alkynylplatinum(II) complexes with 1,3-di(pyrimidin-2-yl)benzene ligands: Synthesis, electrochemistry, photophysics and computational studies. *Dalton Trans.* **2022**, *51*, 5546−5560. (m) Pander, P.; Sil, A.; Salthouse, R. J.; Harris, C. W.; Walden, M. T.; Yufit, D. S.; Williams, J. A. G.; Dias, F. B. Excimer or aggregate? Near infrared electro- and photoluminescence from multimolecular excited states of N^C^N-coordinated platinum(II) complexes. *J. Mater. Chem. C* **2022**, *10*, 15084−15095. (n) Lázaro, A.; Bosque, R.; Ward, J. S.; Rissanen, K.; Crespo, M.; Rodríguez, L. Toward Near-Infrared Emission in Pt(II)-Cyclometallated Compounds: From Excimers' Formation to Aggregation-Induced Emission. *Inorg. Chem.* **2023**, *62*, 2000−2012. (o) Theiss, T.; Buss, S.; Maisuls, I.; López-Arteaga, R.; Brünink, D.; Kösters, J.; Hepp, A.; Doltsinis, N. L.; Weiss, E. A.; Strassert, C. A. Room-Temperature Phosphorescence from Pd(II) and Pt(II) Complexes as Supramolecular Luminophores: The Role of Self-Assembly, Metal-Metal Interactions, Spin-Orbit Coupling, and Ligand-Field Splitting. *J. Am. Chem. Soc.* **2023**, *145*, 3937−3951.
(24) Imai, Y. N.; Inoue, Y.; Nakanishi, I.; Kitaura, K. Cl−π interactions in protein−ligand complexes. *Protein Sci.* **2008**, *17*, 1129−1137.
(25) Indolo[2,3-*b*]indole was prepared by reductive cyclization of 3-(2-nitrophenyl)-1*H*-indole with PPh_3. See: (a) Ai, Q.; Chai, J.; Lou, W.; Liu, T.; Wang, D.; Deng, C.; Wang, C.; Li, G.; Liu, X.; Liu, Z.; Zhang, Q. Efficient and Stable Organic Light-Emitting Diodes Employing Indolo[2,3-*b*]indole-Based Thermally Activated Delayed Fluorescence Emitters. *ACS Appl. Mater. Interfaces* **2020**, *12*, 6127−6136. 3-(2-Nitrophenyl)-1*H*-indole was prepared as reported previously. See: (b) Agarwal, P. K.; Sawant, D.; Sharma, S.; Kundu, B. New Route to the Synthesis of the Isocryptolepine Alkaloid and Its Related Skeletons Using a Modified Pictet-Spengler Reaction. *Eur. J. Org. Chem.* **2009**, *2009*, 292−303.

https://doi.org/10.1021/acs.inorgchem.4c01712
Inorg. Chem. 2024, 63, 14482−14494